HHS Public Access

Author manuscript

Cancer Cell. Author manuscript; available in PMC 2024 December 03.

Published in final edited form as:

Cancer Cell. 2023 September 11; 41(9): 1567–1585.e7. doi:10.1016/j.ccell.2023.07.013.

Integrative multi-omic cancer profiling reveals DNA methylation patterns associated with therapeutic vulnerability and cell-of-origin

Wen-Wei Liang[1,2,‡], **Rita Jui-Hsien Lu**[1,2], **Reyka G. Jayasinghe**[1,2], **Steven M. Foltz**[1,2], **Eduard Porta-Pardo**[3,4], **Yifat Geffen**[5,6], **Michael C. Wendl**[2,7,8], **Rossana Lazcano**[9], **Iga Kolodziejczak**[10,11], **Yizhe Song**[1,2], **Akshay Govindan**[1,2], **Elizabeth G. Demicco**[12], **Xiang Li**[1,2], **Yize Li**[1,2], **Sunantha Sethuraman**[1,2], **Samuel H. Payne**[13], **David Fenyö**[14,15], **Henry Rodriguez**[16], **Maciej Wiznerowicz**[17,18,19], **Hui Shen**[20], **D.R. Mani**[5], **Karin D Rodland**[21,22], **Alexander J. Lazar**[9], **Ana I. Robles**[16], **Li Ding**[1,2,23,24,*], **Clinical Proteomic Tumor Analysis Consortium**

[1]Department of Medicine, Washington University in St. Louis, St. Louis, MO 631110, USA

[2]McDonnell Genome Institute, Washington University in St. Louis, St. Louis, MO 63108, USA

[3]Josep Carreras Leukaemia Research Institute (IJC), Badalona 08916, Spain

[*]Correspondence: lding@wustl.edu (L.D.).

[‡]Current address: New York Genome Center, New York, NY 10013, USA

Secondary author list

François Aguet, Yo Akiyama, Eunkyung An, Shankara Anand, Meenakshi Anurag, Ozgun Babur, Jasmin Bavarva, Chet Birger, Michael Birrer, Anna Calinawan, Lewis C. Cantley, Song Cao, Steve Carr, Michele Ceccarelli, Daniel Chan, Arul Chinnaiyan, Hanbyul Cho, Shrabanti Chowdhury, Marcin Cieslik, Karl Clauser, Antonio Colaprico, Daniel Cui Zhou, Felipe da Veiga Leprevost, Corbin Day, Mohan Dhanasekaran, Marcin Domagalski, Yongchao Dou, Brian Druker, Nathan Edwards, Matthew Ellis, Myvizhi Esai Selvan, Alicia Francis, Gad Getz, Michael A. Gillette, Tania Gonzalez Robles, Sara Gosline, Zeynep Gümüş, David Heiman, Tara Hiltke, Runyu Hong, Galen Hostetter, Yingwei Hu, Chen Huang, Emily Huntsman, Antonio Iavarone, Eric Jaehnig, Scott Jewel, Jiayi Ji, Wen Jiang, Jared Lee Johnson, Lizabeth Katsnelson, Karen Ketchum, Karsten Krug, Chandan Kumar-Sinha, Jonathan Lei, Yuxing Liao, Caleb Lindgren, Tao Liu, Wenke Liu, Weiping Ma, Fernanda Martins Rodrigues, Wilson McKerrow, Mehdi Mesri, Alexey I. Nesvizhskii, Chelsea Newton, Robert Oldroyd, Gilbert Omenn, Amanda Paulovich, Francesca Petralia, Pietro Pugliese, Boris Reva, Kelly Ruggles, Dmitry Rykunov, Shankha Satpathy, Sara Savage, Eric Schadt, Michael Schnaubelt, Tobias Schraink, Zhiao Shi, Dick Smith, Xiaoyu Song, Vasileios Stathias, Erik Storrs, Jimin Tan, Nadezhda Terekhanova, Ratna Thangudu, Mathangi Thiagarajan, Nicole Tignor, Joshua Wang, Liang-Bo Wang, Pei Wang, Ying (Cindy) Wang, Bo Wen, Yige Wu, Lijun Yao, Tomer M. Yaron, Xinpei Yi, Bing Zhang, Hui Zhang, Qing Zhang, Xu Zhang, Zhen Zhang

Authors contributions

Study Conception & Design: W.L., R.J.L., R.J., S.F., L.D.
Performed Experiment or Data Collection: W.L., R.L., I.K., E.D., Y.L., S.S., M.W.
Computational, Multi-omic & Statistical Analyses: W.L, R.J.L., E.P., Y.S., A.G., X.L.
Data Interpretation & Biological Analysis: W.L, R.J.L., R.G.J., S.M.F., E.P., Y.G., R.L., M.W., H.S.
Writing – Original Drafts: W.L. and R.J.L.
Writing – Review & Editing: W.L., R.J.L., R.J., S.F., E.P., Y.G., M.C.W., Y.S., A.G., X.L., Y.L., D.R.M., K.R., A.L., A.R., L.D.
Supervision: W.L. and L.D.
Administration:W.L., S.P., D.F., H.R., D.R.M., K.R., A.L., A.R., L.D.,

Declaration of Interests

The authors declare no competing interests.

Inclusion and diversity

We support inclusive, diverse, and equitable conduct of research.

Declaration of generative AI and AI-assisted technologies in the writing process

During the preparation of this work the author(s) used ChatGPT to enhance its readability. After using this tool/service, the author(s) reviewed and edited the content as needed and take(s) full responsibility for the content of the publication.

[4]Barcelona Supercomputing Center (BSC), Barcelona 08034, Spain

[5]Broad Institute of Massachusetts Institute of Technology and Harvard, Cambridge, MA 02142, USA

[6]Cancer Center and Dept. of Pathology, Massachusetts General Hospital, Boston, MA 02115, USA

[7]Department of Genetics, Washington University in St. Louis, St. Louis, MO 63130, USA

[8]Department of Mathematics, Washington University in St. Louis, St. Louis, MO 63130, USA

[9]Departments of Pathology & Genomic Medicine, The University of Texas MD Anderson Cancer Center, Houston, TX 77030, USA

[10]International Institute for Molecular Oncology, 60-203 Poznań, Poland

[11]Postgraduate School of Molecular Medicine, Medical University of Warsaw, 02-091 Warsaw, Poland

[12]Department of Pathology and Laboratory Medicine, Mount Sinai Hospital and Laboratory Medicine and Pathobiology, University of Toronto, Toronto, ON, Canada

[13]Department of Biology, Brigham Young University, Provo, UT 84602, USA

[14]Institute for Systems Genetics, NYU Grossman School of Medicine, New York, NY 10016, USA

[15]Department of Biochemistry and Molecular Pharmacology, NYU Grossman School of Medicine, New York, NY 10016, USA

[16]Office of Cancer Clinical Proteomics Research, National Cancer Institute, Rockville, MD 20850, USA

[17]International Institute for Molecular Oncology, 60-203 Poznań, Poland

[18]Heliodor Swiecicki Clinical Hospital in Poznań, ul. Przybyszewskiego 49, 60-355 Poznań, Poland

[19]Poznań University of Medical Sciences, 61-701 Poznań, Poland

[20]Van Andel Research Institute, Grand Rapids, MI, 49503, USA

[21]Biological Sciences Division, Pacific Northwest National Laboratory, Richland, WA 99354, USA

[22]Department of Cell, Developmental, and Cancer Biology, Oregon Health & Science University, Portland, OR 97221, USA

[23]Siteman Cancer Center, Washington University in St. Louis, St. Louis, MO 63130, USA

[24]Lead Contact

Summary

DNA methylation plays a critical role in establishing and maintaining cellular identity. However, it is frequently dysregulated during tumor development and is closely intertwined with other genetic alterations. Here, we leveraged multi-omic profiling of 687 tumors and matched non-involved adjacent tissues from kidney, brain, pancreas, lung, head and neck, and endometrium to identify

aberrant methylation associated with RNA and protein abundance changes and build a Pan-Cancer catalog. We uncovered lineage-specific epigenetic drivers including hypomethylated *FGFR2* in endometrial cancer. We showed that hypermethylated *STAT5A* is associated with pervasive regulon downregulation and immune cell depletion, suggesting that epigenetic regulation of *STAT5A* expression constitutes a molecular switch for immunosuppression in squamous tumors. We further demonstrated that methylation subtype-enrichment information can explain cell-of-origin, intra-tumor heterogeneity, and tumor phenotypes. Overall, we identified cis-acting DNA methylation events that drive transcriptional and translational changes, shedding light on the tumor's epigenetic landscape and the role of its cell-of-origin.

eTOC blurb

Liang et al. catalog pan-cancer DNA methylation with concordant transcriptional and translational changes, revealing lineage-specific epigenetic driver *FGFR2* hypomethylation in uterine corpus endometrial carcinoma, and STAT5 hypermethylation as an immunosuppression switch in squamous tumors. They also identify methylation-driven subtypes associated with cell-of-origin, tumor heterogeneity, tumor phenotype, and links to therapeutic potential.

Graphical Abstract

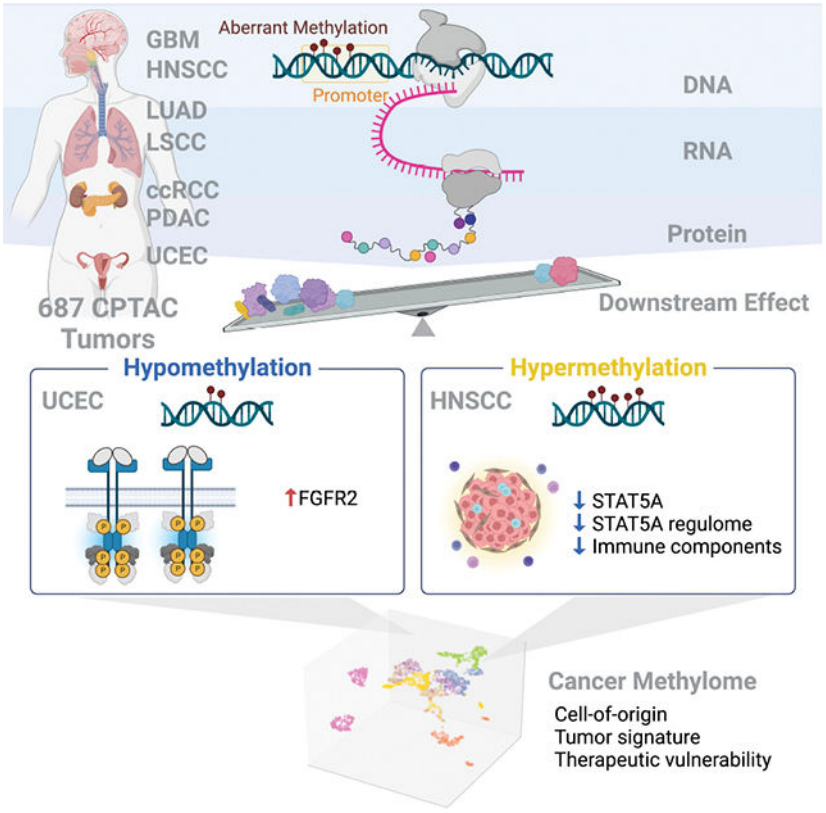

Introduction

Cytosine methylation is an epigenetic modification that confers stability and flexibility in the spatiotemporal gene regulation of many biological processes, including establishment and maintenance of cell identity. Aberrant DNA methylation is a hallmark of human cancer development and progression[1–3]. Aberrant DNA methylation has been observed in the global hypomethylation of repetitive sequences and the gene-specific hypermethylation of numerous CpG islands (CGI)[4,5]. Such changes within promoter regions can silence tumor suppressor genes or deregulate oncogenes. Moreover, the widespread changes in DNA methylation patterns usually arise in the early stages of tumorigenesis, suggesting a driving role of aberrant DNA methylation[6]. Given the reversible and dynamic nature of DNA methylation, treating cells with DNA demethylating agents might reprogram neoplastic cells back toward a normal state[7]. Delineating the functional consequences of aberrant DNA methylation is critical for improving cancer diagnosis, prognosis, and treatment.

Identifying DNA methylation patterns with functional roles in cancer and distinguishing them from tissue-specific epigenetic footprints remains challenging[8]. While some analytical approaches facilitate exploring the connection between DNA methylation and gene expression changes[9,10], most studies have focused solely on transcriptome expression. We propose aggregating multi-omic data to comprehensively understand how tumor-specific methylation impacts both transcription and translation. By leveraging proteomic data as a direct measure of biological activity, we aim to discover DNA methylation drivers and gain insight of their role underlying tumor development.

Here, we integrated multi-omic data from 687 patients across seven cancer types from the Clinical Proteomic Tumor Analysis Consortium (CPTAC)[11], and systematically examined the impact of cis-acting aberrant DNA methylation events on information flow, features, and functional consequences. Our analysis identified common and tissue-specific epigenetic events, including significant alterations in cancer genes affecting hallmark pathways. Distinct cancer subtypes were characterized by unique methylation patterns, validated by RNA and protein signatures reflecting each subtype’s molecular characteristics. Moreover, we identified putative druggable genes tightly regulated by DNA methylation, offering potential targets for tailored therapeutic interventions. This comprehensive catalog advances our understanding of DNA methylation-mediated tumorigenesis and offers insights towards the development of epigenetic therapies.

Results

Pan-Cancer landscape of DNA methylation and associated functional changes

To construct a landscape of cancer methylomes and associated functional changes, we collected 687 human tumors with available DNA methylation profiles (Infinium EPIC array), gene expression (RNA-seq), and protein abundance (mass spectrometry) across seven cancer types from CPTAC. This cohort was comprised of 107 clear cell renal cell carcinomas (ccRCC), 94 glioblastomas (GBM), 104 head and neck squamous cell carcinomas (HNSCC), 107 lung squamous cell carcinomas (LSCC), 102 lung adenocarcinomas (LUAD), 79 pancreatic ductal adenocarcinomas (PDAC), and 94 uterine

corpus endometrial carcinomas (UCEC). We also collected DNA methylation data from matched normal adjacent tissues (NAT) including kidney, head and neck, pancreas, and lung from CPTAC. For GBM and UCEC datasets that lacked DNA methylation data from NATs, we acquired the corresponding DNA methylome from The Cancer Genome Atlas (TCGA) and the Therapeutically Applicable Research to Generate Effective Treatments (TARGET) datasets in the form of Infinium HumanMethylation BeadChip (HM450) (Table S1, STAR Methods). All DNA methylation profiles were processed from raw array data, with standardized processing, quality control, and batch correction procedures (STAR methods). This expanded dataset allowed us to estimate methylation among reference tissues and to interrogate aberrant DNA methylation in a tissue-specific context (Figure S1).

First, to estimate how methylome, transcriptome, and proteome are correlated, we quantified the pairwise correlation between data sets for the 12,943 genes where all measurements are available using linear models, taking into account cancer type and tumor purity as covariates (STAR method, Figure 1A and Table S1). Consistent with expectations, RNA expression positively correlated with protein abundance, and promoter DNA methylation negatively correlated with RNA expression or protein abundance, indicating that promoter hypermethylation leads to gene silencing, while hypomethylation enhances gene expression (Figure 1A). Focusing on the 10,844 genes showing significant mRNA-protein correlation, we categorized them into groups based on the correlation between promoter methylation and RNA/protein expression. The correlation coefficients varied in strength and direction (Figure 1B), with 64.2% of promoter methylation showing no correlation, 18.4% correlated with RNA expression, and 3.5% correlated with protein abundance (Figure 1C). Only 13.9% of the promoter methylation exhibited correlation with both RNA expression and protein abundance (Figure 1C). For example, *MXRA5* and *MNDA* were correlated with RNA expression and protein abundance, respectively, while *CARD11* and *MGMT* showed correlations with both RNA expression and protein abundance (Figure 1D). When parallel correlation tests were conducted within single cancer types without considering tumor purity, the fractions of promoters correlated with both RNA and protein abundance were even lower. This suggests that pan-cancer analysis with a larger sample size enhances discovery power (Table S1).

The limited impact of methylation on the proteome may be attributable to biological factors (e.g., translational regulation, tissue-specific expression, protein degradation, and post-translational modifications) or to technical factors resulting from the low detection sensitivity of low-abundance transcripts or proteins[12,13]. Indeed, we observed a significant decrease in RNA expression and protein abundance in genes where promoter methylation correlated only with RNA expression, compared to those where methylation correlated with both RNA expression and protein abundance (Figure S2A, Wilcoxon $P < 2.2e\text{-}16$). Furthermore, among the 353 genes with promoter methylation correlated solely with protein abundance, we identified 31 genes, including the previously reported *MNDA*[14], with promoter hypermethylation and gene upregulation, indicative of a biological effect rather than a technical artifact (Figure 1D and 1E, Table S1). These genes exhibited enrichment in neutrophil degranulation and glycogen metabolism pathways (Figure 1F and Table S1). The significant correlation between promoter methylation and protein abundance suggests the presence of an additional regulatory layer likely detectable through proteomic data,

emphasizing the intricate and context-specific nature of DNA methylation's impact on gene regulation.

To characterize the prevalence of aberrant DNA methylation across seven cancer types, we next detected recurrent and deregulated DNA methylation in tumors compared to NATs. We then determined the association of DNA methylation with changes in both mRNA expression and protein abundance using the published pipeline RESET[9]. To minimize batch effects or confounding bias across cancer types, each cohort was analyzed individually. Our analysis aimed to profile aberrant DNA methylation for regions actively contributing to gene regulation[15]. Therefore, probe sets were limited to those within promoter regions, or 300 bp upstream and downstream of the transcription start sites for the RESET pipeline (Figure S2B and Table S2). Overall, we detected 5570 hypermethylated CpG sites associated with mRNA downregulation of 2549 genes, 889 hypermethylated CpG sites associated with protein downregulation of 425 genes, 537 hypomethylated CpG sites associated with mRNA upregulation of 442 genes, and 166 hypomethylated CpG sites with protein upregulation of 124 genes (FDR < 10%, Figure 2A). No aberrant DNA methylation has been identified in the PDAC cohort, which could be explained by low tumor purity[16]. Consistent with previous studies, promoter hypermethylation was observed more frequently than promoter hypomethylation in all cancer types[9,17]. Our results confirmed that several well-known tumor-associated genes are regulated epigenetically, including *MLH1* in UCEC[18], *MGMT* in GBM and HNSCC[19]. However, most identified genes have not been previously implicated in DNA methylation-mediated regulation (Table S2).

Next, for individual aberrant DNA methylation events, we examined the concordance between mRNA and protein changes. Out of 964 total hypermethylation and 217 total hypomethylation events, we identified 365 hypermethylation and 74 hypomethylation events associated with both RNA expression and protein abundance changes (Figure 2B and Figure S2C), with a 70.5% validation rate for the genes having available DNA methylation (HM450) and RNA-seq data in TCGA cohorts (FDR < 10%, Table S2). Among them, we observed 98.9% of the aberrant methylation had the same direction of effect across the seven cancer types. About 78.8% of the aberrant methylation have been recovered from the same analysis with tumor purity-adjusted methylation values (FDR < 10%, Table S2), suggesting that our reported events are not being driven by underlying differences in tumor purity. Having constructed a comprehensive map of the cis-acting cancer methylome, we were able to delineate functional impacts of deregulated DNA methylation for a set of genes directly related to tumorigenesis (Table S2). Figure 2C illustrates the median methylation, RNA, and protein differences for cancer-associated genes, presented as the difference between NAT and tumor samples. In line with previous studies, we observed 41 of the aberrant methylation events are cancer type-specific[17,20,21]. Tumor necrosis receptor *FAS* in GBM[22] and homeobox gene *MEIS1* in UCEC[23] are two such examples. Overall, these results highlight the context-dependent regulation of DNA methylation and tissue-specific carcinogenesis[17]. Only 5 of the aberrant methylation events, namely hypomethylated *EGFR*, and hypermethylated *STAT5A, MGMT*, *CARD11*, and *TRIM22* are common across cancer types. The generalizability of these aberrant DNA methylation patterns suggests their importance in tumor development.

Noting that our integrative analysis can also reasonably capture the impact of non-cancerous cells in the tumor microenvironment on bulk multi-omics profiles, we also included published single-cell RNA-seq datasets to annotate whether the reported event is likely to be identified in tumor, immune, or stromal cells[24–28] (STAR methods). For example, in ccRCC, *EGFR* was expressed in cancer cells and *TRIM22* was expressed in immune cells, indicating the possibility of aberrant DNA methylation affecting different populations of cells in the tumor microenvironment. In total, 190 out of 436 events (43.6%) were annotated for their specific expression (Table S2). While our integrative multi-omic analysis based on bulk tissue provides a reliable estimate across a large number of tumors, the complementary scRNA-seq annotations deepen these analyses by evaluating gene expression patterns of the reported events at the cellular level for future study.

cis-acting aberrant DNA methylation as a possible driver event

DNA methylation-mediated modulation might be an important mechanism affecting the regulation of oncogenes and tumor suppressor genes. To test this hypothesis, we characterized cis-acting aberrant DNA methylation on 299 driver genes[29]. Since DNA methylation can affect the binding of transcription factors (TFs)[30], we examined the number and enrichment of TF binding sites (TFBS) in loci associated with expression changes. All loci were associated with at least one TFBS. Both hypomethylated and hypermethylated CGI sites were characterized by a similar number of TFBS (mean 8.14 v.s. 7.49 TFBS) (Figure 3A). PREP1, a master regulator that functions as a tumor suppressor in maintaining genome stability[31], was the most enriched TFBS in hypermethylated loci. This result supports the notion that TFs might serve as both the readers and effectors of aberrant DNA methylation in tumors[30], leading to altered expression as revealed by transcriptomic and proteomic data.

Next, we explored the relationship among genetic alterations, DNA methylation, or histone acetylation. For the driver genes with cis-acting DNA methylations, most methylation events were mutually exclusive with genomic alterations, as exemplified in LSCC (Figure 3B and Figure S3A). For example, the correlation between *KLF5* expression and promoter DNA methylation suggests that methylation is the main factor regulating its expression (Figure S3B). Investigating the interplay between DNA methylation and histone acetylation revealed that tumors exhibiting a high frequency of hypermethylation are significantly linked to decreased levels of H3 acetylation (Figure 3C, Wilcoxon $P<0.05$), indicating an overall repression of genes. Furthermore, a distinct relationship was observed among immune subtypes, hypermethylation frequency, and histone acetylation profiles, where the immune cool group showed an association with tumors displaying high hypermethylation frequency (Figure 3D). The pattern of mutual exclusivity and the interaction between DNA methylation and histone acetylation suggests that DNA methylation contributes to positive selection and histone changes, respectively, potentially playing a driving role in tumorigenesis.

Comparison to NATs showed DNA hypomethylation is the main perturbation occurring in the *IDH2* gene, found in 6 of 107 LSCC tumors (Figure 3E and Figure S3C). Since overexpression of *IDH2* contributes to altered energy metabolism[32,33], we examined the

metabolic activity of those cancers in samples with or without *IDH2* hypomethylation. The results showed preferential upregulation of genes involved in cancer metabolism, including *KDMs*, *ALKBHs*, *TETs*, and *MTOR*, with the specific genes and extent of their expression changes varying slightly across different pathways (Figure 3F). To detect the downstream metabolic remodeling effect of *IDH2* hypomethylation, we investigated the relationship between *IDHs* alterations and histone acetylation profiles. A total of 393 patients with available acetylation and methylation data were categorized into four groups: *IDH1/IDH2* wild-type (n=374), *IDH1* mutants (n=11), IDH2 hypomethylated samples (n=5), and *IDH2* mutants (n=3). We found that *IDH2* hypomethylation, similar to *IDH1* and *IDH2* mutants, can significantly impact the correlations between histone acetylation and DNA methylation levels at 2-hydroxyglutarate (α-KG) target genes (Figure 3G and Table S2) and *IDH2* target genes (Figure S3D and Table S2). For example, significantly lower levels of H1 K168K, H1 K75K, and H2 K86K were observed in *IDH1/2* mutant and *IDH2* hypomethylated samples compared to *IDH1/2* wild types and *IDH2* normal methylated samples, respectively (Figure S3E). Despite the distinct nature of *IDH2* hypomethylation compared to *IDH1* and *IDH2* mutations, the similarity in correlation patterns suggests a potential metabolic convergence of these alterations across cancer types. The combined methylation and acetylation profiling revealed driver mutation-independent *IDH2* activation.

Hypomethylated RTKs are newly identified driver events

We found that several receptor tyrosine kinases (RTKs), including *FGFR2* and *EGFR*, are frequently hypomethylated in UCEC and across cancer types, respectively (Figure 2C). To dissect the contribution of hypomethylated RTKs to oncogene activation, we examined the relationship between promoter methylation and genetic alteration. Specifically, we identified mutations, fusions, and copy number variations (CNVs), and their effects on RTK RNA and protein levels.

About 63.2% (12 of 19) of *FGFR2* missense and indel mutations were activating mutations that enabled high-grade inflammation and cell proliferation without hypomethylation[34–39] (Figure 4A). However, we identified 9 UCEC tumors carrying cis-acting hypomethylated *FGFR2*, 8 of which had co-occurring genomic alterations. Furthermore, unsupervised clustering of DNA methylation data across 94 CPTAC UCEC tumors and 43 TCGA normal samples from the same organ type revealed that *FGFR2* hypomethylated cases formed a distinct cluster with lower DNA methylation than normal tissues (Figure 4B). Specifically, one CGI (cg10314760) within the *FGFR2* promoter displayed a strong correlation between promoter hypomethylation and active gene expression both at the RNA and protein levels (Figure 4C). Our results suggest that promoter methylation is a major factor modulating expression of *FGFR2*, and that *FGFR2* hypomethylation represents another mechanism of RTK activation potentially commensurate with activating mutations.

To distinguish the oncogenic effects of *FGFR2* hypomethylation from co-occurring aberrations, we stratified UCEC tumors by the type of *FGFR2* genomic alteration and examined *FGFR2* expression accordingly. We found that the median of *FGFR2* RNA expression or protein abundance are consistently higher in tumors with hypomethylated *FGFR2* than that in tumors with normal methylated *FGFR2*. Higher expression of *FGFR2*

is significant in the group with CNVs at the cognate locus (Wilcoxon P < 0.005) (Figure 4D). Validation in the TCGA UCEC cohort confirmed our findings. *FGFR2* exhibited hypomethylation at CGI site (cg10314760) in 21 of 174 tumor samples, strongly correlating with active gene expression (Figure S4A). Consistent correlation between *FGFR2* hypomethylation and upregulation was observed in samples with wild type *FGFR2*, shallow deletion of *FGFR2*, and shallow amplification of *FGFR2* (Figure S4B). This result suggests that, whereas activating mutations, amplifications, and promoter hypomethylation enable *FGFR2* upregulation to differing extents, co-occurring *FGFR2* hypomethylated sites result in even more profound expression changes than amplification alone. These results emphasize the important role of promoter hypomethylation in contributing to oncogenic gain-of-function. Similarly, hypomethylated *EGFR* was associated with EGFR upregulation in HNSCC, LSCC, and ccRCC (Figure S4C-D). Our results are consistent with the pan-cancer analysis suggesting that tumors harbor multiple aberrations within individual oncogenes such as *FGFR2* or *EGFR*, likely conferring enhanced oncogenicity in combination[40]. Overall, although recurrent gain-of-function genomic alterations in RTKs have long been known to promote a variety of cancers[41], our results reveal that RTK hypomethylation is also a bona fide epigenetic driver across several cancer types.

Hypermethylation of *STAT5A* is associated with pervasive changes in STAT5A regulon activity

Altered expression of TF can disrupt the activity of its regulon, a group of genes that are regulated by a common regulatory element. To estimate the impact of aberrant DNA methylation on regulon activity, we first identified 14 cis-acting hypermethylation events at TFs, and then tested their association with corresponding regulons, such as receptors, activator, repressor, and target genes involved in the same pathway (Fisher's exact test, FDR P<0.1, Table S3). We identified significant associations between hypermethylated TFs and low regulon activity at both RNA expression and protein abundance levels. Since STAT5A regulon comprises the largest number of interacting genes, we therefore focus on STAT5A for the downstream analysis.

STAT5A controls cell identity, cytotoxicity, and cell survival; dysregulation of those processes can contribute to tumorigenesis[42]. Unsupervised clustering of STAT5A-interacting proteins, using expression data from HNSCC tumors divided samples into two groups: those with high regulon activity and those with low regulon activity (Figure 5A). Notably, samples with hypermethylated *STAT5A* were significantly enriched in the regulon-low group (Fisher's exact test, P=7.8E-05). The same pattern was observed in protein abundance (Figure 5B, Fisher's exact test, P=0.025). Furthermore, exome sequencing of these tumors did not identify any distinct, recurrent coding sequence mutations in STAT5A-interacting genes (Table S3), suggesting that other genetic drivers were not involved. Additionally, STAT5A phosphorylation was not significantly associated with either *STAT5A* methylation status or STAT5A regulon activity (Figure S5A). Altogether, the enrichments we observed indicate that aberrant methylation of *STAT5A* leads to pervasive regulon changes in HNSCC. Similar to HNSCC, hypermethylated *STAT5A* was associated with low regulon activity in LSCC (Figure S5B).

Since samples with hypermethylated *STAT5A* were significantly associated with lower regulon activity at both RNA and protein levels (Figure 5C), we hypothesized that STAT5A-interacting components (i.e., receptors, kinases, repressors, co-activators, and target genes) would be downregulated in samples with hypermethylated *STAT5A*. Among the target genes, we observed significant downregulation of *IRF1*, *PRF1*, *IFNG*, *IL2RA*, and *IL6ST* (Wilcoxon P<0.05) at either/both RNA and protein levels (Figure 5D). These observations link hypermethylated *STAT5A* to the regulation of cytokine production, cytotoxicity, cell proliferation, and interferon signaling.

Hypermethylated *STAT5A* is associated with immune cell depletion in squamous tumors

Recent study has shown that STAT5A-mediated interferon signaling regulates the expression of *CD274* (encodes PD-L1) and *PDCD1LG2* (encodes PD-L2), reflecting the clinical significance of STAT5A signaling in immunotherapy[43]. STAT5A target genes are directly implicated in immune response (e.g., *IL2RA*, *IRF1*, and *IFNG*) and their low expression implies alteration of normal immune function and homeostasis[44]. We therefore focused on characterizing the immune component of HNSCC and LSCC tumors to understand how hypermethylated *STAT5A* affects the tumor microenvironment.

To explore the microenvironment of HNSCC and LSCC tumors, we stratified transcriptome data from cell mixtures into multiple immune cell types using xCell[45]. Consensus clustering of 64 different immune-related cell types identified four major immune clusters, including immune-cold, immune-cool, immune-warm, and immune hot subtypes, which harbored general characteristics of immunosuppressive to inflammatory microenvironment[28,46,47] (Table S3). *STAT5A* hypermethylated samples were significantly enriched in the immune-cool group both in HNSCC and LSCC (Figure 6A and Figure S6A, Fisher's exact test, P<0.00001 and P=0.0002, respectively). *STAT5A* hypermethylated samples displayed significantly decreased expression of genes associated with immune effectors and dendritic cells (Figure 6B and Figure S6B, Wilcoxon P<0.05). Interestingly, for squamous tumors with available histone acetylation data, we found samples with hypermethylated *STAT5A* have significantly lower acetylation of histone H3 lysine 14 (H3K14)(FDR=0.05, Figure S6C), representing an overall gene repression[48]. Our findings suggested that samples with hypermethylated *STAT5A* are significantly associated with immune cell depletion in squamous tumors.

Next, to further identify the expression specificity of *STAT5A* hypermethylation in HNSCC, we evaluated 29 representative HNSCC cases by immunohistochemistry (IHC) markers STAT5A (Table S3). We found prominent STAT5A protein expression in the tumor-infiltrating lymphocytes (TILs) and peritumoral lymphocytes, while STAT5A was minimally expressed or absent in tumor cells (Figure 6C). The overall level of STAT5A abundance in the stained slide was correlated with the level of TILs or peritumoral lymphocytes (Figure 6D). Interestingly, samples with hypermethylated *STAT5A* showed a distinct boundary between tumor cells and STAT5A-expressing immune cells (Figure 6E, left panels), while tumor samples with normal methylated *STAT5A* showed a mixture of tumor cells and STAT5A-expressing immune cells (Figure 6E, right panels). We speculated that immune

cells with hypermethylated *STAT5A* might limit the migration of lymphocytes in the tumor microenvironment, however the working model requires further investigation in the future.

Our finding of lower tumor microenvironment factors in *STAT5A*-hypermethylated samples is in agreement with previous studies showing that hematopoietic stem cell proliferation was severely impaired in *Stat5A*-deficient mice[49–51]. It is also consistent with STAT5A being identified as a key tumor suppressor in lymphoma cell lines[52]. In addition, studies have indicated that the development of HNSCC is closely related to immunosuppression and immune escape[53]. These findings suggest that *STAT5A* hypermethylation may mediate the disease-dependent expression of STAT5A-targeted genes[54] and contributes to altered tumor immunogenicity.

Aberrant methylation associated with therapeutic vulnerabilities

We next explored if epigenetic features can classify tumors into transcriptionally and translationally distinct subtypes. To identify subtypes based on methylation patterns, we generated methylation profiles from 687 tumors and NATs, and used uniform manifold approximation and projection (UMAP) to reduce methylation signals from 340,000 CGIs into two dimensions[55] (Figure 7 and Figure S7A). We found that tumors clustered by organ system, including brain (GBM), kidney (ccRCC), lung (LUAD and LSCC), head and neck (HNSCC), pancreas (PDAC), and uterus (UCEC) (Figure 7A, first column). Additionally, squamous cell cancers, LSCC and HNSCC, formed a distinct cluster adjacent to LUAD. The distinct pattern between chromophobe renal cell carcinomas (C3N-00492 and C3N-01175) and ccRCC samples (Figure S7A) were consistent with their distinct origins[56,57]. Direct comparisons between tumors and corresponding normal adjacent tissues revealed pronounced methylation differences (Figure 7A, second column). To investigate intrinsic lineage differences in DNA methylation between tumors possessing different cells-of-origin, we examined differentially methylated CGIs in tumor samples compared to NAT samples and found 99 cancer-specific aberrant methylation promoters (Figure 7B and Table S4). Together, the results suggest that the DNA methylome of tumors faithfully reflects cell-of-origin and malignant transformation.

Next, using CGIs showing significant differences between tumors and NATs, we identified between 3 and 5 clusters from each cancer type (Figure 7A, third column, and Figure S7B). We correlated those methylation subtypes with existing RNA expression-based subtypes[16,24,56,58–61] (Fisher's exact test $P < 0.05$), and found that methylation subtypes captured several important genomic features and clinical characteristics (Figure S7C and Table S4). For example, the UCEC C1 to C4 methylation subtypes are enriched with POLE, CNV-low, MSI-high, and CNV-high tumors, respectively[62]. The LUAD C1 to C3 methylation subtypes are enriched with proximal-proliferative, proximal-inflammatory, and terminal respiratory unit tumors, respectively[63,64]. GBM subtypes C4 and C5 feature mesenchymal phenotype and CpG island methylator phenotype associated with *IDH1* mutation, respectively[22]. Altogether, our results suggest that clustering cancer samples based on DNA methylation can help identify molecularly and clinically relevant subtypes.

To further explore the biological differences between methylation subtypes, we performed an over-representation pathway analysis using differentially expressed genes and proteins,

revealing significantly enriched pathways related to tumorigenesis (Figure 7C and Table S5, $P < 0.05$). Some significant subtype-specific tumorigenic signatures were consistently observed at the transcriptomic and proteomic levels, such as enrichment of LSCC-C1 for NFE2L2 orchestrating the adaptive response to oxidative stress[65,66], and enrichment of ccRCC-C1 for tumorigenic transcriptional network coordinated by HSF1[67]. Despite comprising distinct cancer types, LSCC-C3, LUAD-C2, PDAC-C2, HNSCC-C2 and GBM-C4 were characterized by immune-related signatures at RNA and/or protein levels. This correlation suggests signaling convergence among various cancers, in line with previous studies demonstrating that some methylation subtypes are significantly associated with immune signature[68–70]. On the other hand, enrichment of pathway signatures was not detected in some methylation subtypes, which were thus only characterized by their distinct methylation pattern. For example, deficiency in DNA polymerase ε (POLE) proofreading generates an extensive number of somatic mutations and leads to a methylation profile, which is shown as the UCEC subtype C1 (Figure 7C and Figure S7D). Overall, these results demonstrate heterogeneity within cancer types and how distinct methylation patterns may give rise to various cancer phenotypes.

To identify the interplay between driver mutation and methylation subtypes in tumorigenesis, we correlated methylation subtypes with 299 driver mutations. We found 13 out of 25 methylation subtypes are significantly associated with cancer-specific driver mutations (Figure 7C and Figure S7D). Consistently, enrichment of seven driver mutations in particular RNA-based subtypes have been identified previously, including UCEC-C4 (CNV-high) enriched with *TP53* mutations[71], UCEC-C3 (MSI-high) with *KMT2B* mutations[61], UCEC-C2 (CNV-low) with *CTNNB1* mutations[71], LUAD-C3 (terminal respiratory unit) with *EGFR* mutations[72], LUAD-C1 (proximal-proliferative) with *STK11* mutations[64], and GBM-C4 (mesenchymal) with *NF1* mutations[73,74]. We also identified enrichment of mutations at epigenetic modifiers that could directly affect cancer methylome. For example, *IDH1* deficiency generates high levels of α-KG and leads to epigenetic reprogramming, which is shown as the GBM subtype C5[24]. Mutations in *PBRM1* (a chromatin remodeler), *SETD2* (a histone methyltransferase), and *BAP1* (a histone deubiquitinating enzyme) lead to distinct DNA methylation phenotypes in ccRCC[75,76]. The significant correlation between driver mutations and methylation subtype suggested that deregulation of driver genes induces epigenetic reprogramming, rewiring regulatory networks together during tumorigenesis.

Beyond the methylation subtyping within each cohort, we also conducted methylation profiling and signature enrichment analysis across HNSCC, LSCC, LUAD, and PDAC, which form a distinct cluster in the UMAP projection (Figure 7A, fourth column, and Figure S7E). We identified six methylation groups with various signatures, including groups enriched with immune-related signatures (MC1 and MC2), groups enriched with squamous tumors (MC3 and MC4), LUAD-dominant group (MC5), and PDAC-dominant group (MC6) (Figure S7F and Table S4, $P < 0.05$). MC5 and MC6 are enriched with cancer type-specific signatures such as β cell development and surfactant metabolism, respectively. Following the observation of methylation subtypes, we again observed signaling convergence among various cancers in MC1 and MC2. Notably, cancers with squamous features (MC3 and MC4) were enriched with replication stress signatures, coinciding with their high degree

of genomic instability[77,78]. Our multi-omic integrative analysis enables the identification of common functionality arising from the same methylation profile across different cancer types.

Finally, we investigated druggable targets for sites with cis-acting dysregulated DNA methylation. We integrated cis-acting DNA methylation with the Clinical Interpretation of Variants in Cancer (CIViC)[79] and analyzed target genes with outlier expressions for which pharmacological intervention might be available (Table S6). Allowing for "off-label" drug treatment, we found that 19.2% of samples (132 of 687 tumors) would likely benefit from one or more treatments targeting genes altered by DNA methylation (Figure S7G). The most frequent druggable DNA methylation events across the seven cancer types are those on *MGMT* (n = 45 tumors), *NAPRT* (n = 31 tumors), and *EGFR* (n = 26 tumors). These findings may have important clinical implications. For example, tumor-specific loss of *NAPRT*, mediated by promoter hypermethylation, is synthetically lethal with NAMPT inhibitor treatment in multiple cancer types, resulting in inactivation of nicotinic acid salvage pathways[80]. However, it is worth mentioning that we do not claim superiority over any other drug discovery method since it is difficult to evaluate the performance without gold standards. We claim that: (1) the high correlation among different data types provides validation to each other for the functional events in tumors; and (2) this study provides highly regulated aberrant DNA methylation events that are reflected in RNA expression and protein abundance readout, which is useful and complementary to other methods. Thus, collectively, these characterizations of cis-acting aberrant DNA methylation in cancer reveal potential new directions for treatment optimization.

Discussion

The pan-cancer multi-omic analysis revealed driver gene regulation via DNA methylation, providing insights into methylation-based stratification of cancer patients. We identified and characterized methylation subtypes enriched with various RNA and protein signatures that have potential therapeutic and prognostic implications. Of interest, we observed that subsets of tumors in different organs may share a convergent immune-related signature. For these, the cancer methylome may offer opportunities for patient stratification to increase the efficacy of immune-based therapies. Moreover, we observed clinically relevant alterations with important therapeutic potential in 132 out of 687 tumors. Targeting those common aberrant methylation events could enhance the therapeutic reach of existing drugs by broadening the treatable patient and tumor populations. To maximize this benefit, future studies may look toward optimizing epigenetic therapies.

We uncovered several bona fide DNA methylation drivers showing functional consequences, including hypomethylated *FGFR2* and *EGFR*, which could be informative in expanding patient eligibility of conventional genotype-directed clinical trials. In addition, the apparent co-occurrence of *FGFR2* hypomethylation and amplification suggests that epigenetic enhancement of *FGFR2* expression may offer selective advantage for developing a second *FGFR2* alteration, perhaps from enhanced FGFR2 signaling in these cells. The converse relationship is also possible: genomic alterations to *FGFR2* disrupt the reading, writing, or maintaining of DNA methylation machinery in tumor cells, subsequently leading to

aberrantly reduced methylation within the *FGFR2* promoter. Regardless of the direction, this relationship takes, since UCEC tumors harboring epigenetic and genetic alterations are significantly associated with *FGFR2* upregulation, it is likely that *FGFR2* hypomethylation works in concert with amplification at *FGFR2* to promote tumorigenesis[81].

Studies have shown that HNSCC tumors evade the host immune system by manipulating their own immunogenicity[53]. Our findings reinforce the critical nature of STAT5A as a signaling hub in modulating tumor immunogenicity across squamous cancers. Together, these findings suggest opportunities for therapeutic intervention by targeting epigenetic alterations within the *STAT5A* promoter. DNMT inhibitors, such as 5'-azacytidine, have been shown to reduce methylation of the *STAT5A* promoter in cell lines[52] and are FDA-approved for treating myelodysplastic syndrome[82]. Furthermore, activation of STAT5A signaling may transform an immunologically cold, inactive tumor into a hot, inflamed one and thus increase the anti-tumor immune response. Additional investigation is required to uncover the mechanisms mediating *STAT5A* hypermethylation and downstream immune-related signaling pathways, including the interaction between them, and the impact on therapeutic sensitivity.

There are several limitations to this study. First, recent investigations have shown that not only promoters, but also intragenic and intergenic regions, are widely modulated during disease progression[83]. Here, we only focus on cis-acting DNA methylation at promoter regions, while trans-acting DNA methylation (i.e. DNA methylation acting upon other target genes) and other regulatory elements are not discussed. Second, previous studies have shown that DNA methylation and gene expression are not as frequently correlated as previously thought[84]. Therefore, DNA methylation may have critical functions other than gene expression regulation. One possibility is that DNA methylation changes influence transcriptional potential rather than actual transcription status and could therefore be involved in the epigenetic plasticity of tumor cells[85,86]. Another possibility is that aberrant intra- or intergenic DNA methylation in cancer cells may lead to increased non-synonymous mutation rate. Finally, although our integrative multi-omic analysis has limitation in differentiating DNA methylation changes specifically in cancer epithelial cells or tumor-infiltrating lymphocytes, we provide a reliable estimate across a wide range of tumors, laying the groundwork for future single-cell analyses and spatial omics investigations. We emphasize the importance of isolating cancer epithelial cells and employing DNA methylome sequencing for future study. Altogether, future studies at single cell resolution may help reveal additional mechanistic details underlying the contribution of aberrant DNA methylation to tumor development.

Overall, our results help identify the contribution of DNA methylation in tumorigenesis and delineate its role in initiating and maintaining malignancies. This thorough account of cis-acting events and characterization of the cancer methylome will inform systematic explorations of aberrant DNA methylation and associated functional consequences, ultimately revealing potential new disease mechanisms and therapeutic opportunities.

Consortia

The members of the National Cancer Institute Clinical Proteomic Tumor Analysis Consortium for Pan-Cancer are François Aguet, Yo Akiyama, Eunkyung An, Shankara Anand, Meenakshi Anurag, Özgün Babur, Jasmin Bavarva, Chet Birger, Michael J. Birrer, Anna Calinawan, Lewis C. Cantley, Song Cao, Steven A. Carr, Michele Ceccarelli, Daniel W. Chan, Arul M. Chinnaiyan, Hanbyul Cho, Shrabanti Chowdhury, Marcin P. Cieslik, Karl R. Clauser, Antonio Colaprico, Daniel Cui Zhou, Felipe da Veiga Leprevost, Corbin Day, Saravana M. Dhanasekaran, Li Ding, Marcin J. Domagalski, Yongchao Dou, Brian J. Druker, Nathan Edwards, Matthew J. Ellis, Myvizhi Esai Selvan, David Fenyö, Steven M. Foltz, Alicia Francis, Yifat Geffen, Gad Getz, Michael A. Gillette, Tania J. Gonzalez Robles, Sara J. C. Gosline, Zeynep H. Gümüş, David I. Heiman, Tara Hiltke, Runyu Hong, Galen Hostetter, Yingwei Hu, Chen Huang, Emily Huntsman, Antonio Iavarone, Eric J. Jaehnig, Scott D. Jewell, Jiayi Ji, Wen Jiang, Jared L. Johnson, Lizabeth Katsnelson, Karen A. Ketchum, Iga Kolodziejczak, Karsten Krug, Chandan Kumar-Sinha, Alexander J. Lazar, Jonathan T. Lei, Yize Li, Wen-Wei Liang, Yuxing Liao, Caleb M. Lindgren, Tao Liu, Wenke Liu, Weiping Ma, D R. Mani, Fernanda Martins Rodrigues, Wilson McKerrow, Mehdi Mesri, Alexey I. Nesvizhskii, Chelsea J. Newton, Robert Oldroyd, Gilbert S. Omenn, Amanda G. Paulovich, Samuel H. Payne, Francesca Petralia, Pietro Pugliese, Boris Reva, Ana I. Robles, Karin D. Rodland, Henry Rodriguez, Kelly V. Ruggles, Dmitry Rykunov, Shankha Satpathy, Sara R. Savage, Eric E. Schadt, Michael Schnaubelt, Tobias Schraink, Stephan Schürer, Zhiao Shi, Richard D. Smith, Xiaoyu Song, Yizhe Song, Vasileios Stathias, Erik P. Storrs, Jimin Tan, Nadezhda V. Terekhanova, Ratna R. Thangudu, Mathangi Thiagarajan, Nicole Tignor, Joshua M. Wang, Liang-Bo Wang, Pei Wang, Ying Wang, Bo Wen, Maciej Wiznerowicz, Yige Wu, Matthew A. Wyczalkowski, Lijun Yao, Tomer M. Yaron, Xinpei Yi, Bing Zhang, Hui Zhang, Qing Zhang, Xu Zhang, Zhen Zhang.

STAR METHODS

RESOURCE AVAILABILITY

Lead contact

- Further information and requests for resources and reagents should be directed to and will be fulfilled by the Lead Contact, Li Ding (lding@wustl.edu).

Materials availability—This study did not generate new unique reagents.

Data and code availability

- Raw and processed proteomics as well as open-access genomic data, can be obtained via Proteomic Data Commons (PDC) at https://pdc.cancer.gov/pdc/cptac-pancancer. Raw genomic and transcriptomic data files can be accessed via the Genomic Data Commons (GDC) Data Portal at https://portal.gdc.cancer.gov with dbGaP Study Accession: phs001287.v16.p6. Complete CPTAC Pan-Cancer controlled and processed data can be accessed via the Cancer Data Service (CDS, https://dataservice.datacommons.cancer.gov/). The CPTAC Pan-Cancer data hosted in CDS is controlled data and can be accessed through the NCI DAC

approved, dbGaP compiled whitelists. Users can access the data for analysis through the Seven Bridges Cancer Genomics Cloud (SB-CGC) which is one of the NCI-funded Cloud Resource/platform for compute intensive analysis. Instructions to access data: 1. Create an account on CGC, Seven Bridges (https://cgc-accounts.sbgenomics.com/auth/register 2. Get approval from dbGaP to access the controlled study (https://www.ncbi.nlm.nih.gov/projects/gap/cgibin/study.cgi?study_id=phs001287. v16.p6) 3. Log into CGC to access Cancer Data Service (CDS) File Explore 4. Copy data into your own space and start analysis and exploration 5. Visit the CDS page on CGC to see what studies are available and instructions and guides to use the resources. (https://docs.cancergenomicscloud.org/page/cds-data).

- All original code has been deposited at GitHub and is publicly available as of the date of publication. DOIs are listed in the key resources table.
- Any additional information required to reanalyze the data reported in this paper is available from the lead contact upon request.

EXPERIMENTAL MODEL AND STUDY PARTICIPANT DETAILS

Human participants—A total of 687 participants were included in strict accordance with the CPTAC-3 protocol with informed consent from the patients. Prospective biospecimen collection (tumor and adjacent normal samples where feasible) followed a tumor type specific protocol and standard operating procedures, where sample collection, qualification and processing were optimized for both genomics and proteomics[16,24,56,58–61]. CPTAC samples were collected by 30+ tissue source sites from both domestic and international locations and processed by a central biospecimen core resource. The samples were pathology qualified by a general pathologist and later reconfirmed by a disease-specific expert pathologist through histopathology image review and immunohistochemistry assays where applicable.

Clinical data annotation—Clinical data were obtained from TSS and aggregated by the Biospecimen Core Resource (BCR, Van Andel Research Institute (Grand Rapids, MI)). Data forms were stored as Microsoft Excel files (.xls). Clinical data can be accessed and downloaded from the CPTAC Data Portal and https://pdc.cancer.gov/pdc/cptac-pancancer as described in [CANCER-CELL-D-22–00603 companion Pan-Cancer resource manuscript][47].

METHODS DETAILS

CPTAC datasets description—We aggregated somatic variants, copy number variations, transcriptomic, proteomic, and clinical data generated by the National Cancer Institute CPTAC from CPTAC data portal, Genomic Data Commons (GDC), and published studies[47] (See Data and Code Availability). The datasets include CPTAC Clear Cell Renal Cell Carcinoma (ccRCC) Discovery Study[56], CPTAC Glioblastoma (GBM) Discovery Study[24], CPTAC Lung Adenocarcinoma (LUAD) Discovery Study[60], CPTAC Lung Squamous Cell Carcinoma (LSCC) Discovery Study[59], CPTAC Head and Neck Cancer (HNSCC) Discovery Study[58], CPTAC Pancreatic Ductal Adenocarcinoma (PDAC) Discovery Study[16], and CPTAC Uterine Corpus Endometrial Carcinoma (UCEC) Discovery Study[61]. Of note,

previous CPTAC cohorts (Breast Invasive Carcinoma, Colon Adenocarcinoma, and Ovarian Serous Cystadenocarcinoma) did not obtain DNA methylation measurement, therefore we could not include those CPTAC cohorts in this study.

All the data were harmonized by CPTAC pipelines[47], which included alignment to the GDC hg38 human reference genome (GRCh38.d1.vd1), annotation with GENCODE v22 (RNA expression quantification) or v34 (the others), and thorough quality checks. Briefly, somatic mutations were called by the SomaticWrapper pipeline from Washington University in St Louis, which includes four different callers: Strelka2[99], MUTECT v1.1.7[100], VarScan v.2.3.8[101], and Pindel v.0.2.5[102]. Copy number variation and structure variants were identified by BIC-seq2[107] and Manta v.1.6.0[108], respectively (CPTAC pipeline from Washington University in St. Louis). Gene fusions in RNA-Seq samples were identified using three callers: STAR-Fusion[104], EricScript[105], and Integrate[106], with fusions reported by at least 2 callers or reported by STAR-Fusion being retained (CPTAC pipeline from Washington University in St Louis)[103]. For transcriptomic data, gene-level stranded read counts were obtained using HTSeq v0.11.2[120] and then converted to Fragments Per Kilobase of transcript per Million mapped reads Upper Quartile (FPKM-UQ) values by following the GDC's RNA-Seq pipeline, except running the quantification tools in the stranded mode (CPTAC pipeline from Washington University in St Louis). Tandem mass tags-based global proteomic and phosphoproteomic data were searched using the MSFragger search engine v3.4[109] against a GENCODE v34 protein FASTA database, processed by Philosopher toolkit v4.0.1[110], and quantified by TMT-Integrator[111]. All the cohorts were uniformly processed and harmonized using the Philosopher toolkit. Missing values for the proteins or phosphosites that appeared in at least 50% of samples were imputed using DreamAI[112] on each cohort separately. The acetylation data for six cancer types (BRCA, GBM, LUAD, LSCC and UCEC) were generated using MS/MS spectra. These spectra were analyzed with Spectrum Mill (SM) v7.08 (proteomics.broadinstitute.org) to identify and quantify the shared acetylation sites among the cohorts.

DNA methylation data preprocessing—Raw methylation image files generated by Illumina Infinium EPIC BeadChip were downloaded from the CPTAC GDC (See Data and Code Availability). We calculated methylated (M) and unmethylated (U) intensities for tumor and normal adjacent tissue samples as described in the methylation processing pipeline on GitHub[121] (See Key Resources Table). Generally, we flagged a locus as NA if probes did not meet a detection P-value of 0.01. Probes with a minor allele frequency more than 0.1 were removed. Probes located on the sex chromosomes and samples with more than 85% NA values were removed from subsequent analysis. Infinium EPIC probes annotated as poor performing were filtered out, leaving 832,749 unique probes[94]. To map EPIC arrays to GRCh38 assembly, all probes are reannotated by InfiniumAnnotation GENCODE v36, which was downloaded from the InfiniumAnnotation website (https://zwdzwd.github.io/InfiniumAnnotation)[94].

The raw methylation image files of TARGET-NBL[88], TCGA-GBM[89], and TCGA-UCEC[71] datasets generated by Illumina Infinium HumanMethylation450 BeadChip assays, used here for normal adjacent tissue approximation, were downloaded from TCGA FireHose or TARGET data matrix and processed as described above. We combined the data derived from

the two platforms, but only used data on common probes (GBM: 364518 probes, UCEC: 364518 probes) (Table S1).

Batch correction of DNA methylation value—To account for batch effects introduced by different data sources, we performed batch-effect correction on the DNA methylation data using the ChAMP Bioconductor package[96] with default parameters. The methylation data matrix was first imputed using the champ.impute() function and then batch-corrected using champ.runCombat() function. Singular value decomposition (SVD) was conducted before and after batch correction for each cohort using champ.SVD() function. The choice of variable for batch correction was determined based on SVD diagnostic plots, where most cancer types were corrected using the "batch" variable, while for GBM and UCEC samples, the "source" variable was utilized. TCGA GBM and TCGA UCEC tumor samples were included solely for the purpose of batch correction and subsequently removed (Table S1). No batch correction was applied to HNSCC samples due to the lack of improvement in SVD diagnostic plots.

Multi-omic data correlation analysis—To investigate the correlation between mean promoter methylation, RNA expression, and protein abundance for 12,934 genes, we utilized linear regression models to fit three different relationships (methylation versus RNA expression, methylation versus protein expression, and RNA expression versus protein expression) and evaluated the significance of each model using adjusted R-squared values, regression coefficients, and P-values of coefficients. Specifically, we used the following model:

$$Y_g = \beta_0 + \beta_1 M_g + \beta_2 P + \beta_3 C + \epsilon$$

where Y is a (n x 1) vector representing either protein or RNA abundance of a given gene, M is a vector indicating the methylation status for that particular gene (g) in a tumor sample, and the tumor purity (P) calculated by ESTIMATE[122] was also included as a covariate. Cancer type was one-hot encoded and was included as an additional covariate (C). Lastly, the error ϵ is assumed to be normally distributed with a constant variance σ.

Additionally, we accounted for multiple comparisons and applied an FDR correction to determine the adjusted P-values and assess the significance of the associations with a threshold of P-value < 0.05. This comprehensive approach enabled us to identify which pairs were significantly associated.

Defining aberrant DNA methylation using RESET—We mapped CpG probes to canonical transcriptional start sites and unconventional exonic TSS as defined by FANTOM5 consortium[87], and then applied the RESET algorithm[9] separately on each tumor type using the corresponding adjacent normal tissue samples. For integrating HM450 (adjacent normal tissue) and EPIC (tumor) datasets for GBM and UCEC, the arrays were intersected to a HM450 probeset to ensure comparability. To identify aberrant DNA methylation events associated with transcriptional or translational changes, aggregated

mRNA expression and global proteomic data were used as an input, respectively. We considered the association as significant if the methylation event had FDR < 10%.

A parallel RESET run was conducted using purity-adjusted beta values. Briefly, a linear regression model is fitted to each tumor cohort using the original methylation estimate as the dependent and “1-purity” as the independent variable to obtain a linear fit, where the resultant intercept is the pure tumor methylation state[123]. After normalizing values between 0 to 1 to satisfy the beta distribution of methylation values, the purity-adjusted beta value at individual CpG sites were obtained. We then repeated our association analysis with purity-adjusted beta values, and provided the mean FDR value in the “FDR_mean|RNA(Purity) “ and “FDR_mean|Protein(Purity)” columns of Table S2 as an additional annotation to the reported events.

For Figure 2C, the methylation difference is derived from the mean beta values differences between samples with or without aberrant methylation. For RNA and protein differences, the values are derived from the mean differences of scaled RNA sequencing data or proteomic data between samples with or without aberrant methylation.

Validation in TCGA cohorts—For aberrant DNA methylation events with concurrent RNA and protein changes where DNA methylation (HM450 array) and RNA-seq data were available from TCGA, we downloaded and uniformly processed the raw DNA methylation data from 2,011 TCGA tumors across 7 cancer types, including ccRCC (N of tumors = 273), GBM (N = 58), HNSCC (N = 514), LSCC (N = 363), LUAD (N = 452), PDAC (N = 177), and UCEC (N = 174). The harmonized RNA expression, protein abundance data (reverse phase protein array, RPPA), mutation profiles, and copy number variation files were downloaded from GDAC. We then identified the aberrant methylation associated with RNA expression or protein abundance changes using the same RESET analysis aforementioned. Since the EPIC array used in this study represents a bigger genomic coverage when compared to the one from TCGA (HM450), we performed a direct comparison of genes where their promoters have been covered in both studies. At least FDR < 10% was required to determine if the event was validated. Due to the sparsity of protein measurements included in the RPPA dataset from TCGA (the mean number of protein measurements in each cohort is 171.1), we calculated the validation rate at RNA level only. The validation results were shown in the “FDR_mean|RNA(TCGA)”, “FDR_mean|Protein(TCGA)”, “No.Methylation.Events_mean|RNA(TCGA)”, and “ProbID|RNA(TCGA)” columns of Table S2.

DEG analysis using scRNA-seq dataset—We used published single-cell RNA-seq (scRNA-seq) datasets[24–27] to annotate whether the reported aberrant DNA methylation event was likely to be identified in cancer cells, immune cells, or stromal cells. Briefly, we separated the cells into three main categories including tumor, immune, and stromal. Differentially expressed genes (DEGs) corresponding to each category were identified by the FindMarkers function in Seurat[124] using the Wilcoxon rank sum test. DEGs were further filtered using the criteria of FDR < 0.05. DEGs identified in the same cancer type with a reported DNA methylation event at the corresponding promoters were annotated in the “scRNA-seq|cluster_matched_cancertype” column of Table S2. DEGs that were uniquely

identified in cancer cells, immune cells, or stromal cells of the other cancer types were annotated in the “scRNA-seq|cluster_cross_cancertype” column of Table S2.

Defining cancer-associated genes—Cancer-associated genes were compiled from a 299 driver gene list defined by Bailey et al[29] and cancer-associated genes listed in Mertins et al[125] and adapted from Vogelstein et al[126].

TFBS enrichment analysis—The frequency distribution of transcription factor bind sites (TFBS) of hypermethylation and hypomethylation probes was conducted at locations of these probes and human hg38 TFBS locations in the JASPAR database[93]. We further defined hyper and hypomethylation significant probes with driver genes and adopted the HOMER software[114] to explore motifs enriched in these significant probes.

Profiling genetic alterations at driver genes—We obtained the somatic mutations in 299 driver genes[29] harboring aberrant DNA methylation as described in “Identification of significantly mutated genes in methylation subtypes”. We further collected gene fusions involved in the driver genes. Aberrant DNA methylation was obtained as described in “Defining aberrant DNA methylation using RESET”. For the CPTAC samples, we defined the log2 copy ratios of each gene larger than 0.3 or smaller than −0.3 as amplification or deletion, respectively. For the TCGA samples, we defined the GISTIC value of −2, −1, 1, 2 as deep deletion, shallow deletion, shallow amplification, and deep amplification, respectively. We separated all the tumors into “No Genomic Alteration”, “Mutation”, and “CNV” categories based on the genomic alteration profiles of the locus being tested. For tumors harboring mutation, CNV, and gene fusions, we categorized them as “Mutation”. The missense mutations at *FGFR2* locus were visualized using ProteintPaint Lollipop.

Histone acetylation analysis—To investigate the impact of *IDH1/2* somatic alterations and aberrant methylations on the correlations between histone acetylation levels and methylation levels at *IDH2* or α-KG target genes, we categorized a total of 393 patients with available acetylation and methylation data into four groups based on their *IDH1/2* mutation and methylation status: *IDH1/IDH2* wild-type (n=374), *IDH1* mutants (n=11), *IDH2* hypomethylated samples (n=5), and *IDH2* mutants (n=3). To assess the levels of histone acetylation and DNA methylation at target genes in each group, we calculated Pearson correlation coefficients and determined the significance levels (P-values) of the correlations using the R function cor.test(). We focused on the acetylation-methylation pairs that showed significant correlations for further analysis (Pearson’s $r > 0.2$, $P < 0.05$, or Pearson’s $r < -0.2$, $P < 0.05$). To examine the differences in correlation coefficients among the groups, we utilized the R package rstatix (version 0.7.2). Specifically, we compared the group differences separately for positively and negatively correlated acetylation-methylation pairs.

We also compared the impact of *IDH1* mutation in GBM and *IDH2* hypomethylation in LSCC on histone acetylation levels. By examining 46 specific sites on histones H1, H2, H3, and H4, we compared the abundance of histone acetylation between *IDH1* mutant (n=7) and wild-type (n=87) groups in GBM, as well as between *IDH2* hypomethylation (n=5) and normal methylation (n=99) groups in LSCC using the Wilcoxon signed-rank test.

Frequency of gene hyper- or hypomethylation—To determine the frequency of hyper- or hypomethylation in each tumor, we calculated the proportion by aggregating the counts of CGI sites exhibiting aberrant methylation and dividing it by the total number of CGI sites in the tumor sample. This analysis was performed using the RESET output.

Regulon association analysis—We collected transcription factor-interacting genes from publicly available databases OmniPath[95], and grouped the samples into regulon-high (>0) and regulon-low (<0) based on the sum of transcription factor-interacting genes using RNA expression and protein abundance data. To test the association of the regulons with the DNA methylation status of transcription factors, we used Fisher's exact test to test for overrepresentation of samples with aberrantly methylated transcription factors in the set of samples defining the regulon activity as described above. To account for multiple comparisons in Fisher's exact test, we applied the Benjamini-Hochberg (BH) method to adjust the P-values for false discovery rate (FDR) control. We narrowed the list of transcription factors down to *STAT5A* and *STAT5A*-interacting genes based on FDR P-value <= 0.1 and the number of interacting genes >=5. We then performed unsupervised clustering of the *STAT5A* regulon using the Ward.D2 linkage method to generate heatmaps.

Cell type enrichment deconvolution—We inferred the abundance of each cell type using the xCell web tool[45] using the FPKM-UQ expression matrix as input. xCell is a gene signature-based method learned from thousands of pure cell types from various sources, which performed the cell type enrichment analysis from gene expression data for 64 immune and stromal cell types (default xCell signature). xCell generates an immune score per sample that integrates the enrichment scores of immune cells (B cells, CD4+ T-cells, CD8+ T-cells, DC, eosinophils, macrophages, monocytes, mast cells, neutrophils, and NK cells), a stroma score, and a micro-environment score which is the sum of the immune score and stroma score[28,47].

Immunohistochemistry analysis—Immunohistochemistry (IHC) staining was performed on 4-micron formalin-fixed, paraffin-embedded (FFPE) tissue sections. Prior to staining, antigen retrieval was performed using the heat-induced epitope retrieval method at pH 6. Staining employed the Dako Autostainer Link 48 with EnVision FLEX visualizing kit (K800221-2; Dako, Agilent Technologies Inc.) and rabbit polyclonal antibody against human STAT5A (HPA042128, Atlas Antibodies, 1:150 dilution). Appropriate known positive and negative control tissue were run in each assay batch.

A semi-quantitative product score for tumor-infiltrating lymphocytes (TILs) and peritumoral lymphocytes were scored by the study pathologists. Percentage of lymphocytes represents the positive lymphocytes relative to the total number of cells (tumors and lymphocytes) in the stained slide, while the intensity represents staining intensity of STAT5A (none, 0; weak, 1; moderate, 2; strong, 3). An independent H-score of STAT5A abundance in the stained slide is calculated using QuPath[115].

Methylation-driven subtyping—To identify subtype based on cancer methylome, we took CGIs showing significant differences between tumors and NATs and performed unsupervised classification of tumors using consensus clustering on the most variable 8,000

CGIs by the R package ConsensusClusterPlus (parameters: reps = 2000, pItem = 0.9, pFeature = 0.9, clusterAlg = “kmdist”, distance = “spearman”)[98]. Samples were assigned to the optimal number of clusters.

Pathway over-representation analysis—To designate the representative pathways of methylation subtypes from transcriptomic and proteomic data, we used the Wilcoxon rank sum test to select the top 250 differentially expressed features (RNA expression and protein abundance) for each subtype or methylation group. We then performed hierarchical clustering on these features. Each set of clustered features underwent pathway enrichment analysis using Reactome[116]. Pathways with P-value smaller than 0.05 were manually reviewed and selected based on the following rules: (1) if similar signatures showed up repeatedly in the significant list, (2) if the significant pathway is supported by literature, and (3) if the signature had been supported by FDR test with P-value smaller than 0.05, (4) if the signatures were consistently observed at the transcriptomic and proteomic levels. Those manually reviewed pathways are highlighted in Figure 7C and Figure S7F.

Identification of significantly mutated genes—A list of 299 driver genes was downloaded from Bailey et al.[29] and results of somatic mutations were downloaded from the CPTAC discovery studies[16,24,56,58–61]. We compiled a genomic alteration profile for each sample (file name: PanCan_Union_Maf_Broad_WashU_v1.1.maf), including frameshift deletion, frameshift insertion, inframe deletion, inframe insertion, missense mutation, nonsense mutation, nonstop mutation, splice site mutation, and intron mutation in 299 driver genes. We then categorized samples with driver mutations based on their methylation subtypes, and conducted Fisher’s exact test to test for overrepresentation of any key driver somatic alterations in the methylation subtypes.

RNA expression-based subtypes—The classifications of RNA expression-based subtypes of ccRCC, GBM, HNSCC, LSCC, LUAD, PDAC, and UCEC samples were downloaded from the CPTAC discovery studies[16,24,58–61]. We then compared the association of RNA expression-based subtype and methylation subtypes using Fisher’s exact test.

Druggable genes with aberrant methylation—CIViC is a curated list of druggable variants describing their therapeutic, prognostic, diagnostic and predisposing relevance. We downloaded the list and intersected the list of genes with aberrant methylation. The potential druggability of each gene was manually reviewed to see if the altered expression of such gene is associated with therapeutic relevance supported by literature.

ADDITIONAL RESOURCES

The CPTAC program website, which includes details about program initiatives, investigators, and datasets, can be accessed at https://proteomics.cancer.gov/programs/cptac.

QUANTIFICATION AND STATISTICAL ANALYSIS

Statistical analysis—All statistical analyses were performed using R or Python unless explained otherwise. Multiple comparisons were adjusted by the Benjamini-Hochberg[127]. Statistical parameters for each experiment are reported in the respective figure legend.

Supplementary Material

Refer to Web version on PubMed Central for supplementary material.

Acknowledgments

We thank InPrint for the editing, Matthew A. Wyczalkowski for feedback on figures, and BioRender for diagrams. The Clinical Proteomic Tumor Analysis Consortium (CPTAC) is supported by the National Cancer Institute of the National Institutes of Health under award numbers U24CA210955, U24CA210985, U24CA210986, U24CA210954, U24CA210967, U24CA210972, U24CA210979, U24CA210993, U01CA214114, U01CA214116, and U01CA214125 as U24CA210972 to D.F., L.D., and S.P., and Contract GR0012005 to L.D. This project has been funded in part with Federal funds from the National Cancer Institute, National Institutes of Health, under Contract No. HHSN261201500003I, Task Order HHSN26100064. The content of this publication does not necessarily reflect the views or policies of the Department of Health and Human Services, nor does mention of trade names, commercial products or organizations imply endorsement by the U.S. Government.

Reference

1. Feinberg AP, Ohlsson R, and Henikoff S. (2006). The epigenetic progenitor origin of human cancer. Nat. Rev. Genet. 7, 21–33. [PubMed: 16369569]
2. Baylin SB, and Jones PA (2011). A decade of exploring the cancer epigenome - biological and translational implications. Nat. Rev. Cancer 11, 726–734. [PubMed: 21941284]
3. Shen H, and Laird PW (2013). Interplay between the cancer genome and epigenome. Cell 153, 38–55. [PubMed: 23540689]
4. Ehrlich M. (2002). DNA methylation in cancer: too much, but also too little. Oncogene 21, 5400–5413. [PubMed: 12154403]
5. Berman BP, Weisenberger DJ, Aman JF, Hinoue T, Ramjan Z, Liu Y, Noushmehr H, Lange CPE, van Dijk CM, Tollenaar RA, et al. (2012). Regions of focal DNA hypermethylation and long-range hypomethylation in colorectal cancer coincide with nuclear lamina--associated domains. Nat. Genet. 44, 40.
6. Easwaran H, Tsai H-C, and Baylin SB (2014). Cancer epigenetics: tumor heterogeneity, plasticity of stem-like states, and drug resistance. Mol. Cell 54, 716–727. [PubMed: 24905005]
7. Ahuja N, Sharma AR, and Baylin SB (2016). Epigenetic Therapeutics: A New Weapon in the War Against Cancer. Annu. Rev. Med. 67, 73–89. [PubMed: 26768237]
8. Kalari S, and Pfeifer GP (2010). Identification of driver and passenger DNA methylation in cancer by epigenomic analysis. Adv. Genet. 70, 277–308. [PubMed: 20920752]
9. Saghafinia S, Mina M, Riggi N, Hanahan D, and Ciriello G. (2018). Pan-Cancer Landscape of Aberrant DNA Methylation across Human Tumors. Cell Rep. 25, 1066–1080.e8. [PubMed: 30355485]
10. Fan S, Tang J, Li N, Zhao Y, Ai R, Zhang K, Wang M, Du W, and Wang W. (2019). Integrative analysis with expanded DNA methylation data reveals common key regulators and pathways in cancers. NPJ Genom Med 4, 2. [PubMed: 30729033]
11. Rodriguez H, Zenklusen JC, Staudt LM, Doroshow JH, and Lowy DR (2021). The next horizon in precision oncology: Proteogenomics to inform cancer diagnosis and treatment. Cell 184, 1661–1670. [PubMed: 33798439]
12. Liu Y, Beyer A, and Aebersold R. (2016). On the Dependency of Cellular Protein Levels on mRNA Abundance. Cell 165, 535–550. [PubMed: 27104977]
13. Buccitelli C, and Selbach M. (2020). mRNAs, proteins and the emerging principles of gene expression control. Nat. Rev. Genet. 10.1038/s41576-020-0258-4.
14. Tang Z, Wang L, Bajinka O, Wu G, and Tan Y. (2022). Abnormal Gene Expression Regulation Mechanism of Myeloid Cell Nuclear Differentiation Antigen in Lung Adenocarcinoma. Biology 11. 10.3390/biology11071047.
15. Ziller MJ, Gu H, Müller F, Donaghey J, Tsai LT-Y, Kohlbacher O, De Jager PL, Rosen ED, Bennett DA, Bernstein BE, et al. (2013). Charting a dynamic DNA methylation landscape of the human genome. Nature 500, 477–481. [PubMed: 23925113]

16. Cao L, Huang C, Cui Zhou D, Hu Y, Lih TM, Savage SR, Krug K, Clark DJ, Schnaubelt M, Chen L, et al. (2021). Proteogenomic characterization of pancreatic ductal adenocarcinoma. Cell 184, 5031–5052.e26. [PubMed: 34534465]
17. Vidal E, Sayols S, Moran S, Guillaumet-Adkins A, Schroeder MP, Royo R, Orozco M, Gut M, Gut I, Lopez-Bigas N, et al. (2017). A DNA methylation map of human cancer at single base-pair resolution. Oncogene 36, 5648–5657. [PubMed: 28581523]
18. Simpkins SB, Bocker T, Swisher EM, Mutch DG, Gersell DJ, Kovatich AJ, Palazzo JP, Fishel R, and Goodfellow PJ (1999). MLH1 promoter methylation and gene silencing is the primary cause of microsatellite instability in sporadic endometrial cancers. Hum. Mol. Genet. 8, 661–666. [PubMed: 10072435]
19. Hegi ME, Diserens A-C, Gorlia T, Hamou M-F, de Tribolet N, Weller M, Kros JM, Hainfellner JA, Mason W, Mariani L, et al. (2005). MGMT gene silencing and benefit from temozolomide in glioblastoma. N. Engl. J. Med. 352, 997–1003. [PubMed: 15758010]
20. Hansen KD, Timp W, Bravo HC, Sabunciyan S, Langmead B, McDonald OG, Wen B, Wu H, Liu Y, Diep D, et al. (2011). Increased methylation variation in epigenetic domains across cancer types. Nat. Genet. 43, 768–775. [PubMed: 21706001]
21. Witte T, Plass C, and Gerhauser C. (2014). Pan-cancer patterns of DNA methylation. Genome Med. 6, 66. [PubMed: 25473433]
22. Noushmehr H, Weisenberger DJ, Diefes K, Phillips HS, Pujara K, Berman BP, Pan F, Pelloski CE, Sulman EP, Bhat KP, et al. (2010). Identification of a CpG island methylator phenotype that defines a distinct subgroup of glioma. Cancer Cell 17, 510–522. [PubMed: 20399149]
23. Yang F, Liu D, Deng Y, Wang J, Mei S, Ge S, Li H, Zhang C, and Zhang T. (2020). Frequent promoter methylation of HOXD10 in endometrial carcinoma and its pathological significance. Oncol. Lett. 19, 3602–3608. [PubMed: 32269635]
24. Wang L-B, Karpova A, Gritsenko MA, Kyle JE, Cao S, Li Y, Rykunov D, Colaprico A, Rothstein JH, Hong R, et al. (2021). Proteogenomic and metabolomic characterization of human glioblastoma. Cancer Cell. 10.1016/j.ccell.2021.01.006.
25. Li Y, Lih T-SM, Dhanasekaran SM, Mannan R, Chen L, Cieslik M, Wu Y, Lu RJ-H, Clark DJ, Kołodziejczak I, et al. (2022). Histopathologic and proteogenomic heterogeneity reveals features of clear cell renal cell carcinoma aggressiveness. Cancer Cell. 10.1016/j.ccell.2022.12.001.
26. Cui Zhou D, Jayasinghe RG, Chen S, Herndon JM, Iglesia MD, Navale P, Wendl MC, Caravan W, Sato K, Storrs E, et al. (2022). Spatially restricted drivers and transitional cell populations cooperate with the microenvironment in untreated and chemo-resistant pancreatic cancer. Nat. Genet. 54, 1390–1405. [PubMed: 35995947]
27. Travaglini KJ, Nabhan AN, Penland L, Sinha R, Gillich A, Sit RV, Chang S, Conley SD, Mori Y, Seita J, et al. (2020). A molecular cell atlas of the human lung from single-cell RNA sequencing. Nature 587, 619–625. [PubMed: 33208946]
28. CPTAC (2023). Companion Pan-Cancer Driver paper. Cell.
29. Bailey MH, Tokheim C, Porta-Pardo E, Sengupta S, Bertrand D, Weerasinghe A, Colaprico A, Wendl MC, Kim J, Reardon B, et al. (2018). Comprehensive Characterization of Cancer Driver Genes and Mutations. Cell 173, 371–385.e18. [PubMed: 29625053]
30. Zhu H, Wang G, and Qian J. (2016). Transcription factors as readers and effectors of DNA methylation. Nat. Rev. Genet. 17, 551–565. [PubMed: 27479905]
31. Iotti G, Longobardi E, Masella S, Dardaei L, De Santis F, Micali N, and Blasi F. (2011). Homeodomain transcription factor and tumor suppressor Prep1 is required to maintain genomic stability. Proc. Natl. Acad. Sci. U. S. A. 108, E314–22. [PubMed: 21715654]
32. Li J, He Y, Tan Z, Lu J, Li L, Song X, Shi F, Xie L, You S, Luo X, et al. (2018). Wild-type IDH2 promotes the Warburg effect and tumor growth through HIF1α in lung cancer. Theranostics 8, 4050–4061. [PubMed: 30128035]
33. Bergaggio E, and Piva R. (2019). Wild-Type IDH Enzymes as Actionable Targets for Cancer Therapy. Cancers 11. 10.3390/cancers11040563.
34. Yu K, Herr AB, Waksman G, and Ornitz DM (2000). Loss of fibroblast growth factor receptor 2 ligand-binding specificity in Apert syndrome. Proc. Natl. Acad. Sci. U. S. A. 97, 14536–14541. [PubMed: 11121055]

35. Pollock PM, Gartside MG, Dejeza LC, Powell MA, Mallon MA, Davies H, Mohammadi M, Futreal PA, Stratton MR, Trent JM, et al. (2007). Frequent activating FGFR2 mutations in endometrial carcinomas parallel germline mutations associated with craniosynostosis and skeletal dysplasia syndromes. Oncogene 26, 7158–7162. [PubMed: 17525745]
36. Gartside MG, Chen H, Ibrahimi OA, Byron SA, Curtis AV, Wellens CL, Bengston A, Yudt LM, Eliseenkova AV, Ma J, et al. (2009). Loss-of-function fibroblast growth factor receptor-2 mutations in melanoma. Mol. Cancer Res. 7, 41–54. [PubMed: 19147536]
37. Byron SA, Chen H, Wortmann A, Loch D, Gartside MG, Dehkhoda F, Blais SP, Neubert TA, Mohammadi M, and Pollock PM (2013). The N550K/H mutations in FGFR2 confer differential resistance to PD173074, dovitinib, and ponatinib ATP-competitive inhibitors. Neoplasia 15, 975–988. [PubMed: 23908597]
38. Liao RG, Jung J, Tchaicha J, Wilkerson MD, Sivachenko A, Beauchamp EM, Liu Q, Pugh TJ, Pedamallu CS, Hayes DN, et al. (2013). Inhibitor-sensitive FGFR2 and FGFR3 mutations in lung squamous cell carcinoma. Cancer Res. 73, 5195–5205. [PubMed: 23786770]
39. Ng PK-S, Li J, Jeong KJ, Shao S, Chen H, Tsang YH, Sengupta S, Wang Z, Bhavana VH, Tran R, et al. (2018). Systematic Functional Annotation of Somatic Mutations in Cancer. Cancer Cell 33, 450–462.e10. [PubMed: 29533785]
40. Saito Y, Koya J, Araki M, Kogure Y, Shingaki S, Tabata M, McClure MB, Yoshifuji K, Matsumoto S, Isaka Y, et al. (2020). Landscape and function of multiple mutations within individual oncogenes. Nature 582, 95–99. [PubMed: 32494066]
41. Robertson SC, Tynan J, and Donoghue DJ (2000). RTK mutations and human syndromes: when good receptors turn bad. Trends Genet. 16, 368. [PubMed: 10904266]
42. Rani A, and Murphy JJ (2016). STAT5 in Cancer and Immunity. J. Interferon Cytokine Res. 36, 226–237. [PubMed: 26716518]
43. Garcia-Diaz A, Shin DS, Moreno BH, Saco J, Escuin-Ordinas H, Rodriguez GA, Zaretsky JM, Sun L, Hugo W, Wang X, et al. (2017). Interferon Receptor Signaling Pathways Regulating PD-L1 and PD-L2 Expression. Cell Rep. 19, 1189–1201. [PubMed: 28494868]
44. Platanias LC (2005). Mechanisms of type-I- and type-II-interferon-mediated signalling. Nat. Rev. Immunol. 5, 375–386. [PubMed: 15864272]
45. Aran D, Hu Z, and Butte AJ (2017). xCell: digitally portraying the tissue cellular heterogeneity landscape. Genome Biol. 18, 220. [PubMed: 29141660]
46. CPTAC (2023). Companion PTM paper.
47. CPTAC (2023). Companion Pan-Cancer Resource paper.
48. Karmodiya K, Krebs AR, Oulad-Abdelghani M, Kimura H, and Tora L. (2012). H3K9 and H3K14 acetylation co-occur at many gene regulatory elements, while H3K14ac marks a subset of inactive inducible promoters in mouse embryonic stem cells. BMC Genomics 13, 424. [PubMed: 22920947]
49. Zhang S, Fukuda S, Lee Y, Hangoc G, Cooper S, Spolski R, Leonard WJ, and Broxmeyer HE (2000). Essential role of signal transducer and activator of transcription (Stat)5a but not Stat5b for Flt3-dependent signaling. J. Exp. Med. 192, 719–728. [PubMed: 10974037]
50. Yao Z, Cui Y, Watford WT, Bream JH, Yamaoka K, Hissong BD, Li D, Durum SK, Jiang Q, Bhandoola A, et al. (2006). Stat5a/b are essential for normal lymphoid development and differentiation. Proc. Natl. Acad. Sci. U. S. A. 103, 1000–1005. [PubMed: 16418296]
51. Park J-H, Adoro S, Guinter T, Erman B, Alag AS, Catalfamo M, Kimura MY, Cui Y, Lucas PJ, Gress RE, et al. (2010). Signaling by intrathymic cytokines, not T cell antigen receptors, specifies CD8 lineage choice and promotes the differentiation of cytotoxic-lineage T cells. Nat. Immunol. 11, 257–264. [PubMed: 20118929]
52. Zhang Q, Wang HY, Liu X, and Wasik MA (2007). STAT5A is epigenetically silenced by the tyrosine kinase NPM1-ALK and acts as a tumor suppressor by reciprocally inhibiting NPM1-ALK expression. Nat. Med. 13, 1341–1348. [PubMed: 17922009]
53. Ferris RL (2015). Immunology and Immunotherapy of Head and Neck Cancer. J. Clin. Oncol. 33, 3293–3304. [PubMed: 26351330]
54. Villarino AV, Kanno Y, and O'Shea JJ (2017). Mechanisms and consequences of Jak-STAT signaling in the immune system. Nat. Immunol. 18, 374–384. [PubMed: 28323260]

55. McInnes L, Healy J, Saul N, and Großberger L. (2018). UMAP: Uniform Manifold Approximation and Projection. Journal of Open Source Software 3, 861. 10.21105/joss.00861.
56. Clark DJ, Dhanasekaran SM, Petralia F, Pan J, Song X, Hu Y, da Veiga Leprevost F, Reva B, Lih T-SM, Chang H-Y, et al. (2019). Integrated Proteogenomic Characterization of Clear Cell Renal Cell Carcinoma. Cell 179, 964–983.e31. [PubMed: 31675502]
57. Davis CF, Ricketts CJ, Wang M, Yang L, Cherniack AD, Shen H, Buhay C, Kang H, Kim SC, Fahey CC, et al. (2014). The somatic genomic landscape of chromophobe renal cell carcinoma. Cancer Cell 26, 319–330. [PubMed: 25155756]
58. Huang C, Chen L, Savage SR, Eguez RV, Dou Y, Li Y, da Veiga Leprevost F, Jaehnig EJ, Lei JT, Wen B, et al. (2021). Proteogenomic insights into the biology and treatment of HPV-negative head and neck squamous cell carcinoma. Cancer Cell 39, 361–379.e16. [PubMed: 33417831]
59. Satpathy S, Krug K, Jean Beltran PM, Savage SR, Petralia F, Kumar-Sinha C, Dou Y, Reva B, Kane MH, Avanessian SC, et al. (2021). A proteogenomic portrait of lung squamous cell carcinoma. Cell 184, 4348–4371.e40. [PubMed: 34358469]
60. Gillette MA, Satpathy S, Cao S, Dhanasekaran SM, Vasaikar SV, Krug K, Petralia F, Li Y, Liang W-W, Reva B, et al. (2020). Proteogenomic Characterization Reveals Therapeutic Vulnerabilities in Lung Adenocarcinoma. Cell 182, 200–225.e35. [PubMed: 32649874]
61. Dou Y, Kawaler EA, Cui Zhou D, Gritsenko MA, Huang C, Blumenberg L, Karpova A, Petyuk VA, Savage SR, Satpathy S, et al. (2020). Proteogenomic Characterization of Endometrial Carcinoma. Cell 180, 729–748.e26. [PubMed: 32059776]
62. Sanchez-Vega F, Mina M, Armenia J, Chatila WK, Luna A, La KC, Dimitriadoy S, Liu DL, Kantheti HS, Saghafinia S, et al. (2018). Oncogenic Signaling Pathways in The Cancer Genome Atlas. Cell 173, 321–337.e10. [PubMed: 29625050]
63. Wilkerson MD, Yin X, Walter V, Zhao N, Cabanski CR, Hayward MC, Miller CR, Socinski MA, Parsons AM, Thorne LB, et al. (2012). Differential pathogenesis of lung adenocarcinoma subtypes involving sequence mutations, copy number, chromosomal instability, and methylation. PLoS One 7, e36530.
64. Cancer Genome Atlas Research Network (2014). Comprehensive molecular profiling of lung adenocarcinoma. Nature 511, 543–550. [PubMed: 25079552]
65. Jeong Y, Hoang NT, Lovejoy A, Stehr H, Newman AM, Gentles AJ, Kong W, Truong D, Martin S, Chaudhuri A, et al. (2017). Role of KEAP1/NRF2 and TP53 Mutations in Lung Squamous Cell Carcinoma Development and Radiation Resistance. Cancer Discov. 7, 86–101. [PubMed: 27663899]
66. Ryoo I-G, and Kwak M-K (2018). Regulatory crosstalk between the oxidative stress-related transcription factor Nfe2l2/Nrf2 and mitochondria. Toxicol. Appl. Pharmacol. 359, 24–33. [PubMed: 30236989]
67. Mendillo ML, Santagata S, Koeva M, Bell GW, Hu R, Tamimi RM, Fraenkel E, Ince TA, Whitesell L, and Lindquist S. (2012). HSF1 drives a transcriptional program distinct from heat shock to support highly malignant human cancers. Cell 150, 549–562. [PubMed: 22863008]
68. Wauters E, Janssens W, Vansteenkiste J, Decaluwé H, Heulens N, Thienpont B, Zhao H, Smeets D, Sagaert X, Coolen J, et al. (2015). DNA methylation profiling of non-small cell lung cancer reveals a COPD-driven immune-related signature. Thorax 70, 1113–1122. [PubMed: 26349763]
69. Hoadley KA, Yau C, Hinoue T, Wolf DM, Lazar AJ, Drill E, Shen R, Taylor AM, Cherniack AD, Thorsson V, et al. (2018). Cell-of-Origin Patterns Dominate the Molecular Classification of 10,000 Tumors from 33 Types of Cancer. Cell 173, 291–304.e6. [PubMed: 29625048]
70. Pereira B, Billaud M, and Almeida R. (2017). RNA-Binding Proteins in Cancer: Old Players and New Actors. Trends Cancer Res. 3, 506–528.
71. Cancer Genome Atlas Research Network, Kandoth C, Schultz N, Cherniack AD, Akbani R, Liu Y, Shen H, Robertson AG, Pashtan I, Shen R, et al. (2013). Integrated genomic characterization of endometrial carcinoma. Nature 497, 67–73. [PubMed: 23636398]
72. Yatabe Y, Kosaka T, Takahashi T, and Mitsudomi T. (2005). EGFR mutation is specific for terminal respiratory unit type adenocarcinoma. Am. J. Surg. Pathol. 29, 633–639. [PubMed: 15832087]
73. Verhaak RGW, Hoadley KA, Purdom E, Wang V, Qi Y, Wilkerson MD, Miller CR, Ding L, Golub T, Mesirov JP, et al. (2010). Integrated genomic analysis identifies clinically relevant subtypes of

glioblastoma characterized by abnormalities in PDGFRA, IDH1, EGFR, and NF1. Cancer Cell 17, 98–110. [PubMed: 20129251]

74. Phillips HS, Kharbanda S, Chen R, Forrest WF, Soriano RH, Wu TD, Misra A, Nigro JM, Colman H, Soroceanu L, et al. (2006). Molecular subclasses of high-grade glioma predict prognosis, delineate a pattern of disease progression, and resemble stages in neurogenesis. Cancer Cell 9, 157–173. [PubMed: 16530701]
75. Tiedemann RL, Hlady RA, Hanavan PD, Lake DF, Tibes R, Lee J-H, Choi J-H, Ho TH, and Robertson KD (2016). Dynamic reprogramming of DNA methylation in SETD2-deregulated renal cell carcinoma. Oncotarget 7, 1927–1946. [PubMed: 26646321]
76. Chen Y-C, Gotea V, Margolin G, and Elnitski L. (2017). Significant associations between driver gene mutations and DNA methylation alterations across many cancer types. PLoS Comput. Biol. 13, e1005840.
77. Papalouka C, Adamaki M, Batsaki P, Zoumpourlis P, Tsintarakis A, Goulielmaki M, Fortis SP, Baxevanis CN, and Zoumpourlis V. (2023). DNA Damage Response Mechanisms in Head and Neck Cancer: Significant Implications for Therapy and Survival. Int. J. Mol. Sci. 24. 10.3390/ijms24032760.
78. Cancer Genome Atlas Research Network (2012). Comprehensive genomic characterization of squamous cell lung cancers. Nature 489, 519–525. [PubMed: 22960745]
79. Griffith M, Spies NC, Krysiak K, McMichael JF, Coffman AC, Danos AM, Ainscough BJ, Ramirez CA, Rieke DT, Kujan L, et al. (2017). CIViC is a community knowledgebase for expert crowdsourcing the clinical interpretation of variants in cancer. Nat. Genet. 49, 170–174. [PubMed: 28138153]
80. Shames DS, Elkins K, Walter K, Holcomb T, Du P, Mohl D, Xiao Y, Pham T, Haverty PM, Liederer B, et al. (2013). Loss of NAPRT1 expression by tumor-specific promoter methylation provides a novel predictive biomarker for NAMPT inhibitors. Clin. Cancer Res. 19, 6912–6923. [PubMed: 24097869]
81. Saito Y, Koya J, and Kataoka K. (2021). Multiple mutations within individual oncogenes. Cancer Sci. 112, 483–489. [PubMed: 33073435]
82. Tsai H-C, Li H, Van Neste L, Cai Y, Robert C, Rassool FV, Shin JJ, Harbom KM, Beaty R, Pappou E, et al. (2012). Transient low doses of DNA-demethylating agents exert durable antitumor effects on hematological and epithelial tumor cells. Cancer Cell 21, 430–446. [PubMed: 22439938]
83. Shenker N, and Flanagan JM (2012). Intragenic DNA methylation: implications of this epigenetic mechanism for cancer research. Br. J. Cancer 106, 248–253. [PubMed: 22166804]
84. Spainhour JC, Lim HS, Yi SV, and Qiu P. (2019). Correlation Patterns Between DNA Methylation and Gene Expression in The Cancer Genome Atlas. Cancer Inform. 18, 1176935119828776.
85. Raynal NJ-M, Si J, Taby RF, Gharibyan V, Ahmed S, Jelinek J, Estécio MRH, and Issa J-PJ (2012). DNA methylation does not stably lock gene expression but instead serves as a molecular mark for gene silencing memory. Cancer Res. 72, 1170–1181. [PubMed: 22219169]
86. Flavahan WA, Gaskell E, and Bernstein BE (2017). Epigenetic plasticity and the hallmarks of cancer. Science 357. 10.1126/science.aal2380.
87. FANTOM Consortium and the RIKEN PMI and CLST (DGT), Forrest, A.R.R., Kawaji H, Rehli M, Baillie JK, de Hoon MJL, Haberle V, Lassmann T, Kulakovskiy IV, Lizio M, et al. (2014). A promoter-level mammalian expression atlas. Nature 507, 462–470. [PubMed: 24670764]
88. Pugh TJ, Morozova O, Attiyeh EF, Asgharzadeh S, Wei JS, Auclair D, Carter SL, Cibulskis K, Hanna M, Kiezun A, et al. (2013). The genetic landscape of high-risk neuroblastoma. Nat. Genet. 45, 279–284. [PubMed: 23334666]
89. Brennan CW, Verhaak RGW, McKenna A, Campos B, Noushmehr H, Salama SR, Zheng S, Chakravarty D, Sanborn JZ, Berman SH, et al. (2013). The somatic genomic landscape of glioblastoma. Cell 155, 462–477. [PubMed: 24120142]
90. Cancer Genome Atlas Research Network (2013). Comprehensive molecular characterization of clear cell renal cell carcinoma. Nature 499, 43–49. [PubMed: 23792563]
91. Cancer Genome Atlas Research Network. Electronic address: andrew_aguirre@dfci.harvard.edu, and Cancer Genome Atlas Research Network (2017). Integrated Genomic Characterization of Pancreatic Ductal Adenocarcinoma. Cancer Cell 32, 185–203.e13. [PubMed: 28810144]

92. Cancer Genome Atlas Network (2015). Comprehensive genomic characterization of head and neck squamous cell carcinomas. Nature 517, 576–582. [PubMed: 25631445]

93. Khan A, Fornes O, Stigliani A, Gheorghe M, Castro-Mondragon JA, van der Lee R, Bessy A, Chèneby J, Kulkarni SR, Tan G, et al. (2018). JASPAR 2018: update of the open-access database of transcription factor binding profiles and its web framework. Nucleic Acids Res. 46, D260–D266. [PubMed: 29140473]

94. Zhou W, Laird PW, and Shen H. (2017). Comprehensive characterization, annotation and innovative use of Infinium DNA methylation BeadChip probes. Nucleic Acids Res. 45, e22. [PubMed: 27924034]

95. Türei D, Korcsmáros T, and Saez-Rodriguez J. (2016). OmniPath: guidelines and gateway for literature-curated signaling pathway resources. Nat. Methods 13, 966–967. [PubMed: 27898060]

96. Morris TJ, Butcher LM, Feber A, Teschendorff AE, Chakravarthy AR, Wojdacz TK, and Beck S. (2014). ChAMP: 450k Chip Analysis Methylation Pipeline. Bioinformatics 30, 428–430. [PubMed: 24336642]

97. Maksimovic J, Phipson B, and Oshlack A. (2016). A cross-package Bioconductor workflow for analysing methylation array data. F1000Res. 5, 1281. [PubMed: 27347385]

98. Wilkerson MD, and Hayes DN (2010). ConsensusClusterPlus: a class discovery tool with confidence assessments and item tracking. Bioinformatics 26, 1572–1573. [PubMed: 20427518]

99. Saunders CT, Wong WSW, Swamy S, Becq J, Murray LJ, and Cheetham RK (2012). Strelka: accurate somatic small-variant calling from sequenced - sample pairs. Bioinformatics 28, 1811–1817. [PubMed: 22581179]

100. Cibulskis K, Lawrence MS, Carter SL, Sivachenko A, Jaffe D, Sougnez C, Gabriel S, Meyerson M, Lander ES, and Getz G. (2013). Sensitive detection of somatic point mutations in impure and heterogeneous cancer samples. Nat. Biotechnol. 31, 213–219. [PubMed: 23396013]

101. Koboldt DC, Zhang Q, Larson DE, Shen D, McLellan MD, Lin L, Miller CA, Mardis ER, Ding L, and Wilson RK (2012). VarScan 2: somatic mutation and copy number alteration discovery in cancer by exome sequencing. Genome Res. 22, 568–576. [PubMed: 22300766]

102. Ye K, Schulz MH, Long Q, Apweiler R, and Ning Z. (2009). Pindel: a pattern growth approach to detect break points of large deletions and medium sized insertions from paired-end short reads. Bioinformatics 25, 2865–2871. [PubMed: 19561018]

103. Gao Q, Liang W-W, Foltz SM, Mutharasu G, Jayasinghe RG, Cao S, Liao W-W, Reynolds SM, Wyczalkowski MA, Yao L, et al. (2018). Driver Fusions and Their Implications in the Development and Treatment of Human Cancers. Cell Rep. 23, 227–238.e3. [PubMed: 29617662]

104. Haas BJ, Dobin A, Li B, Stransky N, Pochet N, and Regev A. (2019). Accuracy assessment of fusion transcript detection via read-mapping and de novo fusion transcript assembly-based methods. Genome Biol. 20, 213. [PubMed: 31639029]

105. Benelli M, Pescucci C, Marseglia G, Severgnini M, Torricelli F, and Magi A. (2012). Discovering chimeric transcripts in paired-end RNA-seq data by using EricScript. Bioinformatics 28, 3232–3239. [PubMed: 23093608]

106. Zhang J, White NM, Schmidt HK, Fulton RS, Tomlinson C, Warren WC, Wilson RK, and Maher CA (2016). INTEGRATE: gene fusion discovery using whole genome and transcriptome data. Genome Res. 26, 108–118. [PubMed: 26556708]

107. Xi R, Lee S, Xia Y, Kim T-M, and Park PJ (2016). Copy number analysis of whole-genome data using BIC-seq2 and its application to detection of cancer susceptibility variants. Nucleic Acids Res. 44, 6274–6286. [PubMed: 27260798]

108. Chen X, Schulz-Trieglaff O, Shaw R, Barnes B, Schlesinger F, Källberg M, Cox AJ, Kruglyak S, and Saunders CT (2016). Manta: rapid detection of structural variants and indels for germline and cancer sequencing applications. Bioinformatics 32, 1220–1222. [PubMed: 26647377]

109. Kong AT, Leprevost FV, Avtonomov DM, Mellacheruvu D, and Nesvizhskii AI (2017). MSFragger: ultrafast and comprehensive peptide identification in mass spectrometry-based proteomics. Nat. Methods 14, 513–520. [PubMed: 28394336]

110. da Veiga Leprevost F, Haynes SE, Avtonomov DM, Chang H-Y, Shanmugam AK, Mellacheruvu D, Kong AT, and Nesvizhskii AI (2020). Philosopher: a versatile toolkit for shotgun proteomics data analysis. Nat. Methods 17, 869–870. [PubMed: 32669682]

111. Djomehri SI, Gonzalez ME, da Veiga Leprevost F, Tekula SR, Chang H-Y, White MJ, Cimino-Mathews A, Burman B, Basrur V, Argani P, et al. (2020). Quantitative proteomic landscape of metaplastic breast carcinoma pathological subtypes and their relationship to triple-negative tumors. Nat. Commun. 11, 1723. [PubMed: 32265444]
112. Ma W, Kim S, Chowdhury S, Li Z, Yang M, Yoo S, Petralia F, Jacobsen J, Li JJ, Ge X, et al. (2020). DreamAI: algorithm for the imputation of proteomics data. bioRxiv, 2020.07.21.214205. 10.1101/2020.07.21.214205.
113. Ritchie ME, Phipson B, Wu D, Hu Y, Law CW, Shi W, and Smyth GK (2015). limma powers differential expression analyses for RNA-sequencing and microarray studies. Nucleic Acids Res. 43, e47. [PubMed: 25605792]
114. Heinz S, Benner C, Spann N, Bertolino E, Lin YC, Laslo P, Cheng JX, Murre C, Singh H, and Glass CK (2010). Simple combinations of lineage-determining transcription factors prime cis-regulatory elements required for macrophage and B cell identities. Mol. Cell 38, 576–589. [PubMed: 20513432]
115. Bankhead P, Loughrey MB, Fernández JA, Dombrowski Y, McArt DG, Dunne PD, McQuaid S, Gray RT, Murray LJ, Coleman HG, et al. (2017). QuPath: Open source software for digital pathology image analysis. Sci. Rep. 7, 16878. [PubMed: 29203879]
116. Fabregat A, Sidiropoulos K, Viteri G, Forner O, Marin-Garcia P, Arnau V, D'Eustachio P, Stein L, and Hermjakob H. (2017). Reactome pathway analysis: a high-performance in-memory approach. BMC Bioinformatics 18, 142. [PubMed: 28249561]
117. Wolf FA, Angerer P, and Theis FJ (2018). SCANPY: large-scale single-cell gene expression data analysis. Genome Biol. 19, 15. [PubMed: 29409532]
118. Grüning B, Dale R, Sjödin A, Chapman BA, Rowe J, Tomkins-Tinch CH, Valieris R, Köster J, and Bioconda Team (2018). Bioconda: sustainable and comprehensive software distribution for the life sciences. Nat. Methods 15, 475–476. [PubMed: 29967506]
119. Huber W, Carey VJ, Gentleman R, Anders S, Carlson M, Carvalho BS, Bravo HC, Davis S, Gatto L, Girke T, et al. (2015). Orchestrating high-throughput genomic analysis with Bioconductor. Nat. Methods 12, 115–121. [PubMed: 25633503]
120. Anders S, Pyl PT, and Huber W. (2015). HTSeq--a Python framework to work with high-throughput sequencing data. Bioinformatics 31, 166–169. [PubMed: 25260700]
121. Fortin J-P, Labbe A, Lemire M, Zanke BW, Hudson TJ, Fertig EJ, Greenwood CM, and Hansen KD (2014). Functional normalization of 450k methylation array data improves replication in large cancer studies. Genome Biol. 15, 503. [PubMed: 25599564]
122. Yoshihara K, Shahmoradgoli M, Martínez E, Vegesna R, Kim H, Torres-Garcia W, Treviño V, Shen H, Laird PW, Levine DA, et al. (2013). Inferring tumour purity and stromal and immune cell admixture from expression data. Nat. Commun. 4, 2612. [PubMed: 24113773]
123. Staaf J, and Aine M. (2022). Tumor purity adjusted beta values improve biological interpretability of high-dimensional DNA methylation data. PLoS One 17, e0265557.
124. Hao Y, Hao S, Andersen-Nissen E, Mauck WM 3rd, Zheng S, Butler A, Lee MJ, Wilk AJ, Darby C, Zager M, et al. (2021). Integrated analysis of multimodal single-cell data. Cell 184, 3573–3587.e29. [PubMed: 34062119]
125. Mertins P, Mani DR, Ruggles KV, Gillette MA, Clauser KR, Wang P, Wang X, Qiao JW, Cao S, Petralia F, et al. (2016). Proteogenomics connects somatic mutations to signalling in breast cancer. Nature 534, 55–62. [PubMed: 27251275]
126. Vogelstein B, Papadopoulos N, Velculescu VE, Zhou S, Diaz LA Jr, and Kinzler KW (2013). Cancer genome landscapes. Science 339, 1546–1558. [PubMed: 23539594]
127. Benjamini Y, and Hochberg Y. (1995). Controlling the false discovery rate: A practical and powerful approach to multiple testing. J. R. Stat. Soc. 57, 289–300.

Highlights

1. Pan-cancer epigenetic aberrations and their transcriptional and translational changes
2. *FGFR2* and *EGFR* hypomethylation are bona fide driver DNA methylation events.
3. *STAT5A* methylation is a potential switch for immunosuppression in squamous tumors.
4. Methylation subtypes illuminate cell origin, tumor heterogeneity, and tumor phenotype.

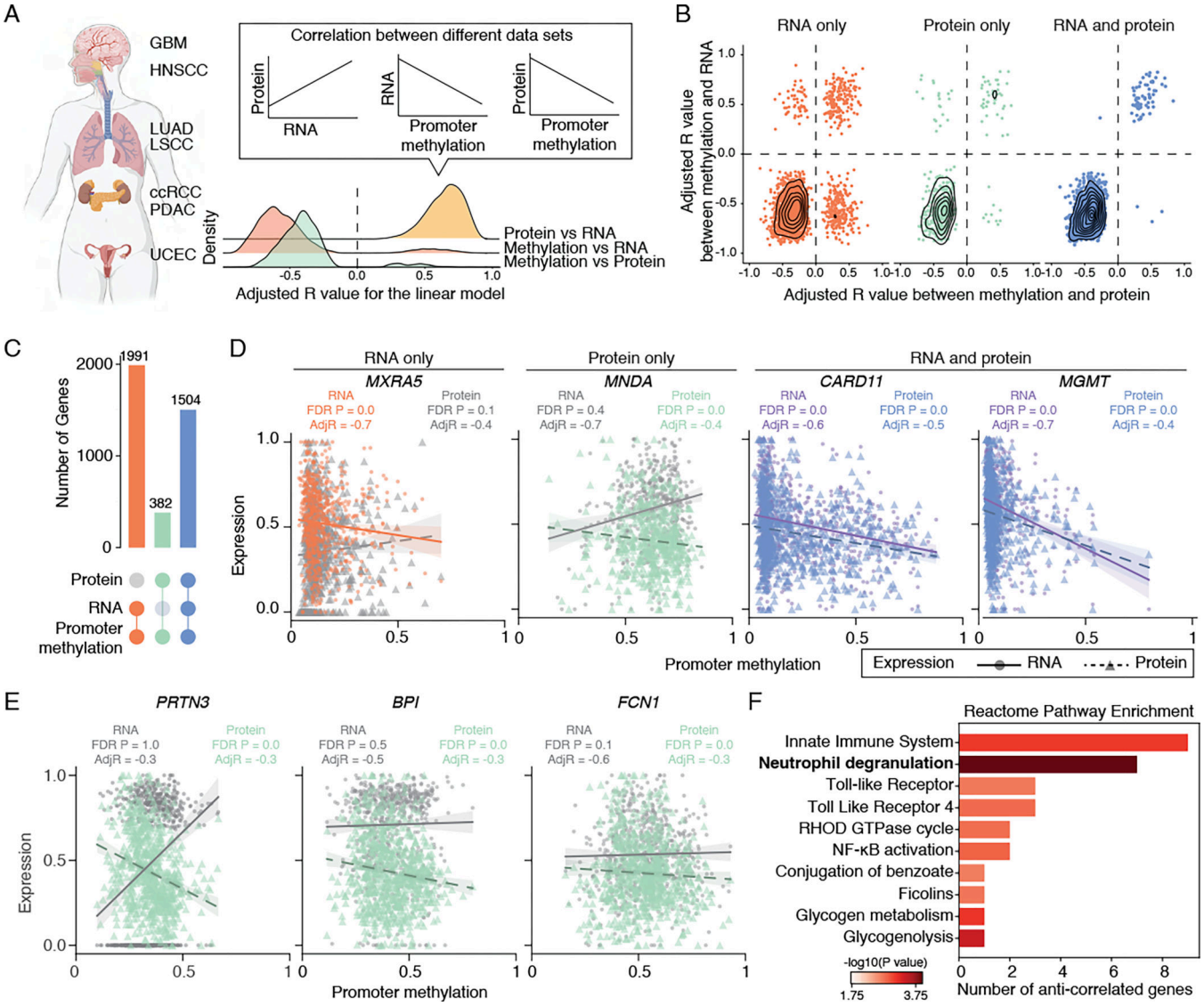

Figure 1. Correlations between promoter DNA methylation, transcriptome, and proteome

(A) Left: A schematic of tumor types collected for this study. Right: Density plot showing the distribution of adjusted R values between protein abundance and RNA expression (yellow), promoter methylation and RNA expression (orange) or protein abundance (green).

(B) Scatter plot showing adjusted R values distribution for genes with promoter methylation correlated with RNA (left, orange), protein (middle, green), or both RNA and protein (right, blue).

(C) Upsetplot showing the breakdown of genes based on their correlation with promoter methylation and RNA/protein expression.

(D) Examples with distinct correlations between promoter methylation, RNA expression, and protein abundance. Each dot represents one tumor, with the solid line representing the correlation between scaled RNA and promoter methylation, and the dashed line representing the correlation between scaled protein abundance and promoter methylation. Significant

correlations are highlighted (orange: RNA only; green: protein only, blue and purple: RNA and protein).

(E) Examples of anti-correlated genes with promoter hypermethylation, exhibiting upregulation at the RNA level and downregulation at the protein level.

(F) Pathway enrichment analysis of the 31 anti-correlated genes with promoter hypermethylation, showing upregulation at the RNA level and downregulation at the protein level. Pathway with FDR P-value <0.05 is highlighted in bold.

See also Figures S1, S2, and Table S1.

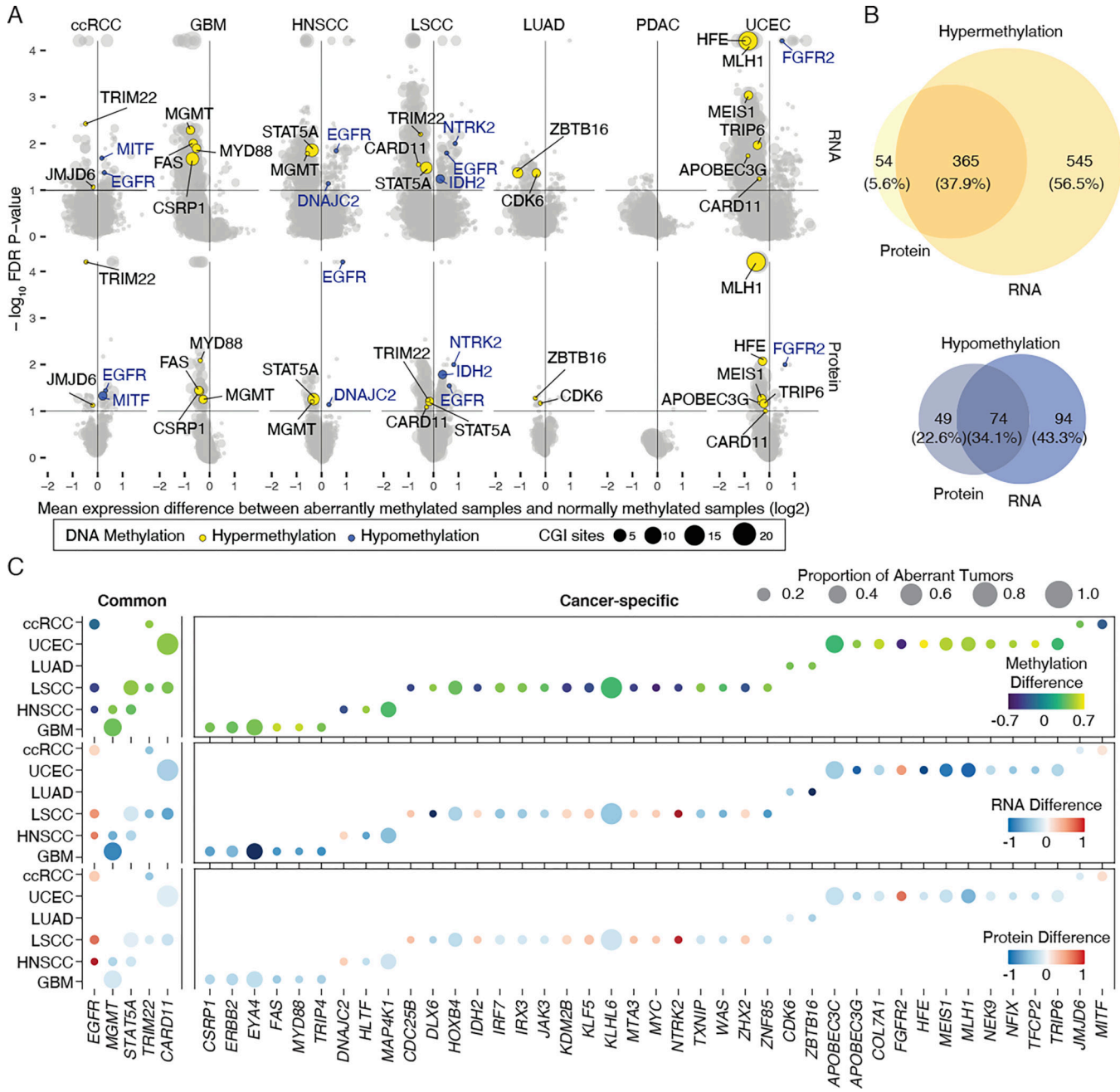

Figure 2. The cancer methylome landscape associated with transcriptomic and proteomic change

(A) RNA expression (upper) and protein abundance (lower) changes in genes between aberrant and normal samples. Y axis corresponds to the statistical significance of aberrant DNA methylation with changed expression and x axis to the median difference of gene expression of samples with or without aberrant DNA methylation. Representative genes are colored based on methylation status: yellow, hypermethylation; blue, hypomethylation. Dot size indicates the number of CGIs associated with expression changes.

(B) Venn diagrams showing the number of hypermethylated (upper) and hypomethylated (lower) genes having significant RNA expression and/or protein abundance changes.

(C) Common and cancer type-specific aberrant methylations of cancer-associated genes. Shading of the filled circle indicates the median methylation difference (upper), RNA expression difference (middle), and protein abundance difference (lower) between aberrant and normal samples at significant CpG sites. Dot size is proportional to the number of samples harboring indicated aberrant DNA methylation events in the cancer cohort. See also Figure S2 and Table S2.

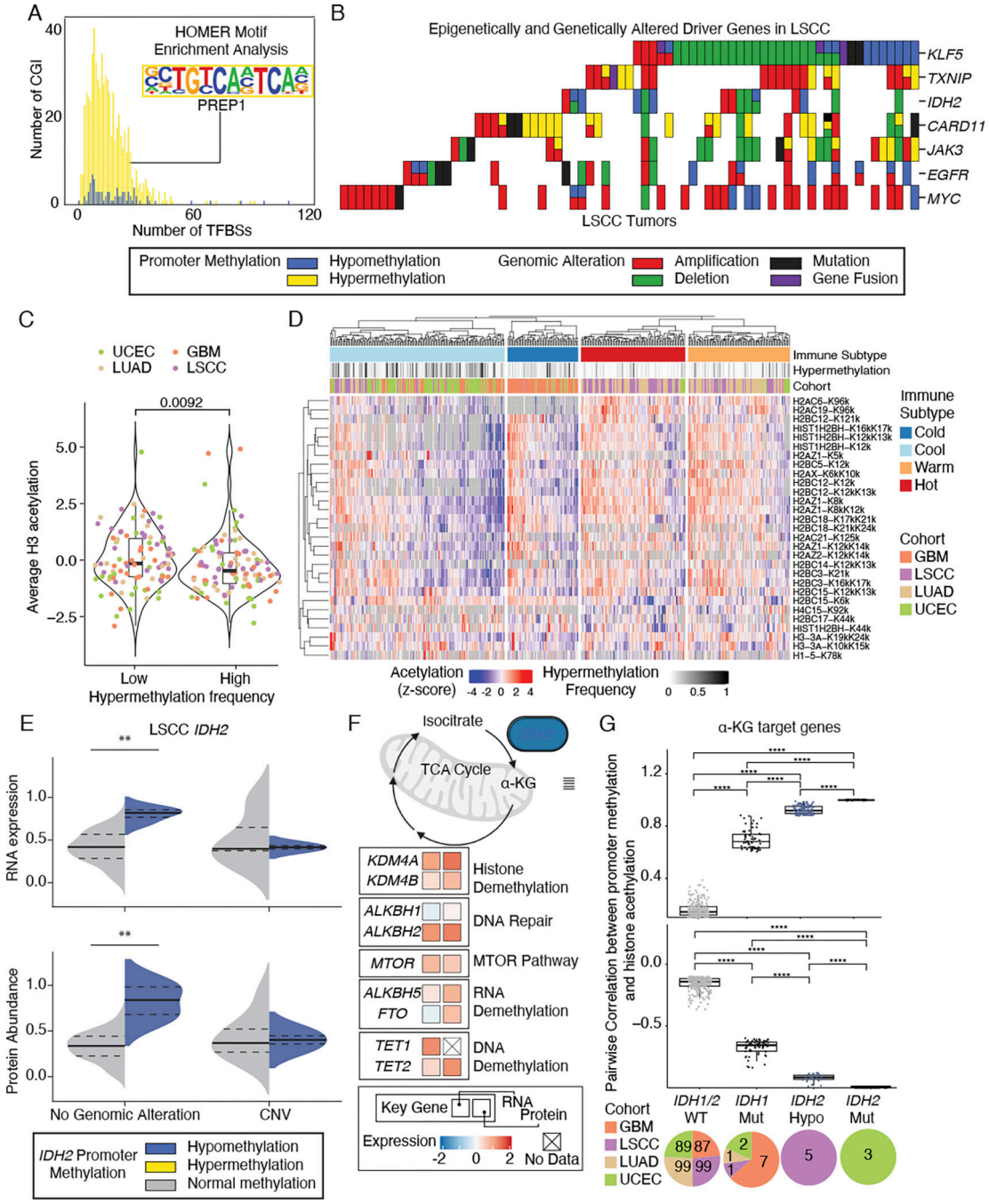

Figure 3. Characterization of aberrant methylation in driver genes

(A) Distribution of the number of transcription factor binding sites for functional hypermethylation (yellow) and hypomethylation (blue). Enriched motif was highlighted in the inset.

(B) Mutual exclusivity and co-occurrence of genomic and epigenomic alterations in driver genes in LSCC.

(C) Violin plot comparing histone H3 acetylation levels between highly hypermethylated tumors and lowly hypermethylated tumors. Boxes represent the interquartile range (IQR),

with the median frequency indicated by the horizontal line. Whiskers extend from the boxes to indicate the data range. Statistically significant differences between groups were determined using Wilcoxon rank sum test.

(D) Heatmap of histone sites exhibiting significant differential acetylation (FDR < 0.1) among immune subtypes. The grayscale color scale denotes the hypermethylation frequency in each tumor.

(E) RNA expression (upper) and protein abundance (lower) levels stratified by *IDH2* genomic alterations and *IDH2* hypomethylation (blue) versus *IDH2* normal methylation (gray), with ** denoting Wilcoxon P<0.005. Median values are shown as solid black lines, and first and third quartiles are represented by dashed lines.

(F) Pathway diagram illustrating the average difference in RNA expression (left square) and protein abundance (right square) between *IDH2* hypomethylated samples and normal methylated samples in LSCC. The shading of the filled squares indicates the extent of the differences.

(G) Positive (upper) and negative (lower) correlation coefficients of histone acetylation levels and methylation levels at α-KG target genes among *IDH1/IDH2* wild-type, *IDH1* mutant, *IDH2* hypomethylated samples, and *IDH2* mutant. The breakdown of each group was shown in the pie chart below. Boxes represent the IQR, with the median correlation value indicated by the horizontal line. Whiskers extend from the boxes to show the data range. Statistically significant differences between groups were determined using FDR-corrected P-values, with **** indicating P < 2.2e-16.

See also Figure S3 and Table S2.

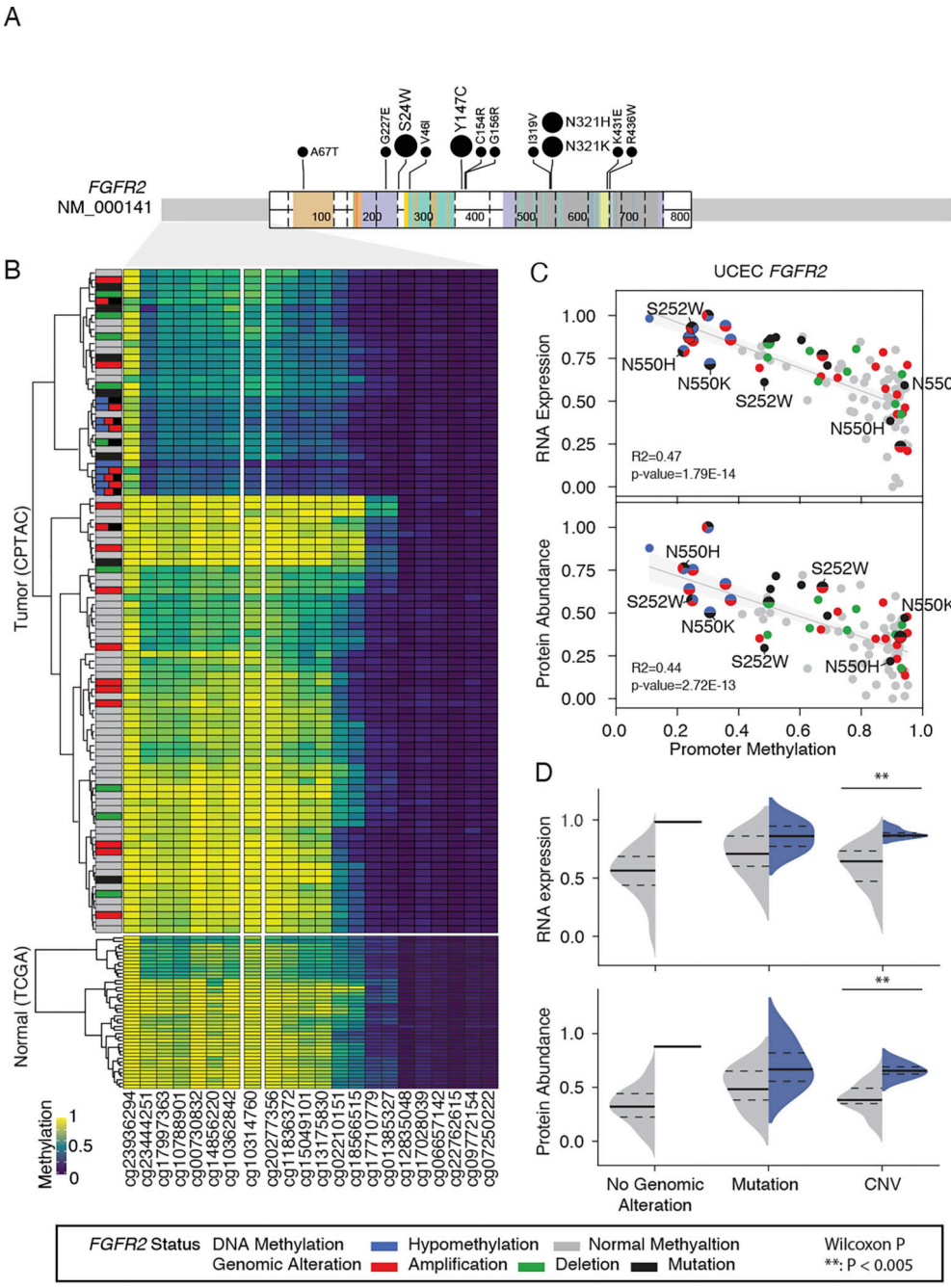

Figure 4. Collaborative effects of *FGFR2* mutations and hypomethylation on *FGFR2* upregulation

(A) Lolliplot showing missense mutations of *FGFR2* in UCEC samples. The amino acids and types of mutations are labeled. Positions that are recurrently mutated are highlighted with the number of occurrences. The *FGFR2* functional domains are colored.

(B) Unsupervised clustering of UCEC tumors (upper) and normal adjacent tissues (lower) based on DNA methylation of the *FGFR2* promoter.

(C) Correlation of methylation with gene expression (upper) and protein abundance (lower). Samples are colored based on genetic and/or epigenetic alterations of *FGFR2*. Tumors harboring *FGFR2* hypomethylation are highlighted by large dot size.
(D) RNA expression (upper) and protein abundance (lower) levels stratified by *FGFR2* genomic alterations and *FGFR2* hypomethylation (blue) versus *FGFR2* normal methylation (gray), with ** denoting Wilcoxon P<0.005. Median values are shown as solid black lines, and first and third quartiles are represented by dashed lines.
See also Figure S4.

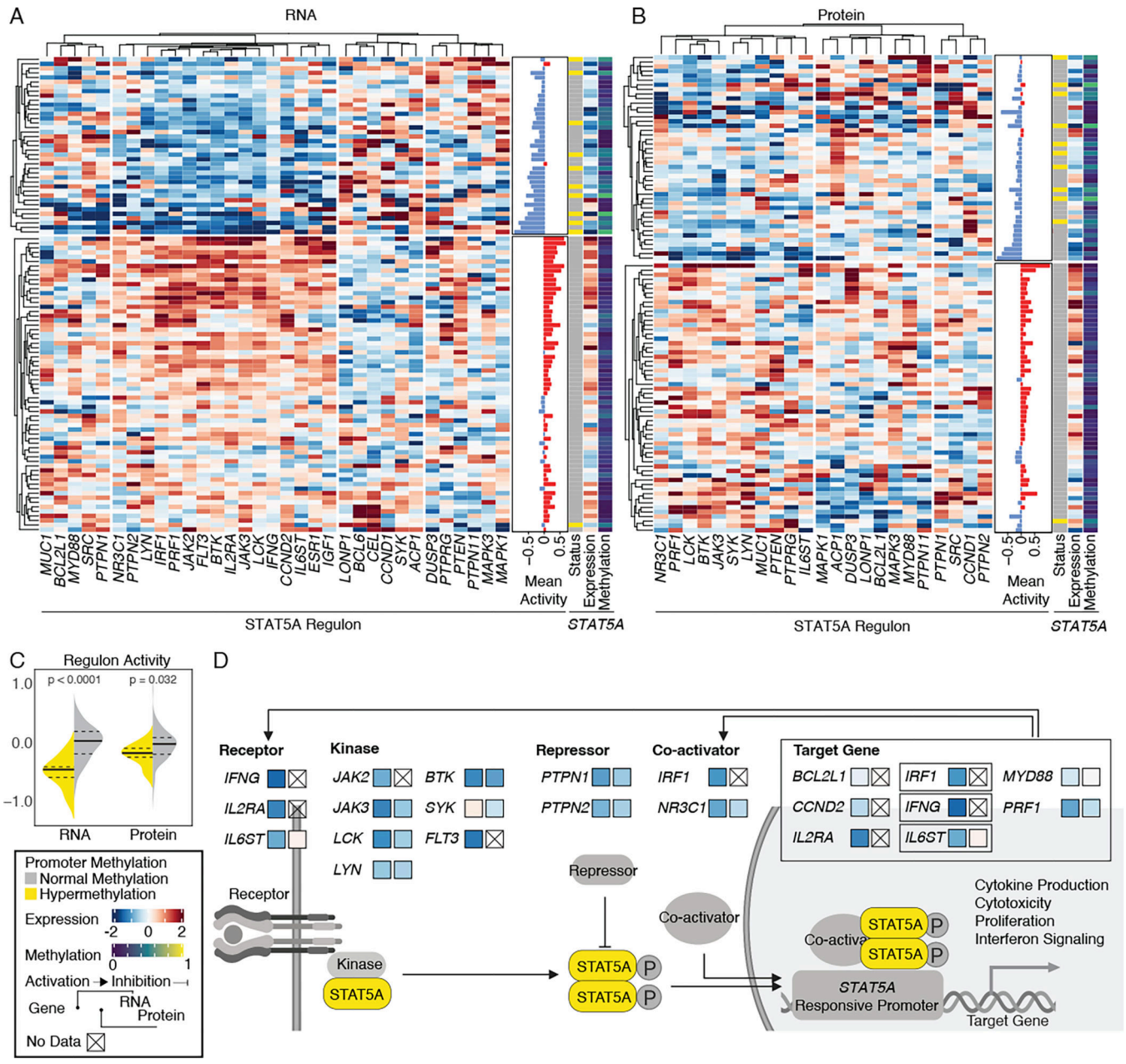

Figure 5. *STAT5A* hypermethylation associated with pervasive STAT5A regulon changes

(A) Unsupervised clustering of STAT5A regulon genes using Pearson correlation of scaled RNA sequencing data. Annotations denote *STAT5A* expression and methylation levels. Mean activity indicates the overall sum of regulon activity. The color scale is proportional to expression (red: upregulation; blue: downregulation).

(B) Unsupervised clustering of STAT5A regulon genes using Pearson correlation of scaled global proteome data.

(C) Violin plot comparing regulon activity in hypermethylated STAT5A (yellow) and normally methylated STAT5A (gray) samples. Median values are shown as solid black lines,

and first and third quartiles are represented by dashed lines. Statistical significance was determined using a Wilcoxon rank-sum test.

(D) Pathway members and interactions in the STAT5A regulon. The mean expression differences between *STAT5A* hypermethylated samples and normally methylated samples are indicated by shading of the filled squares.

See also Figure S5 and Table S3.

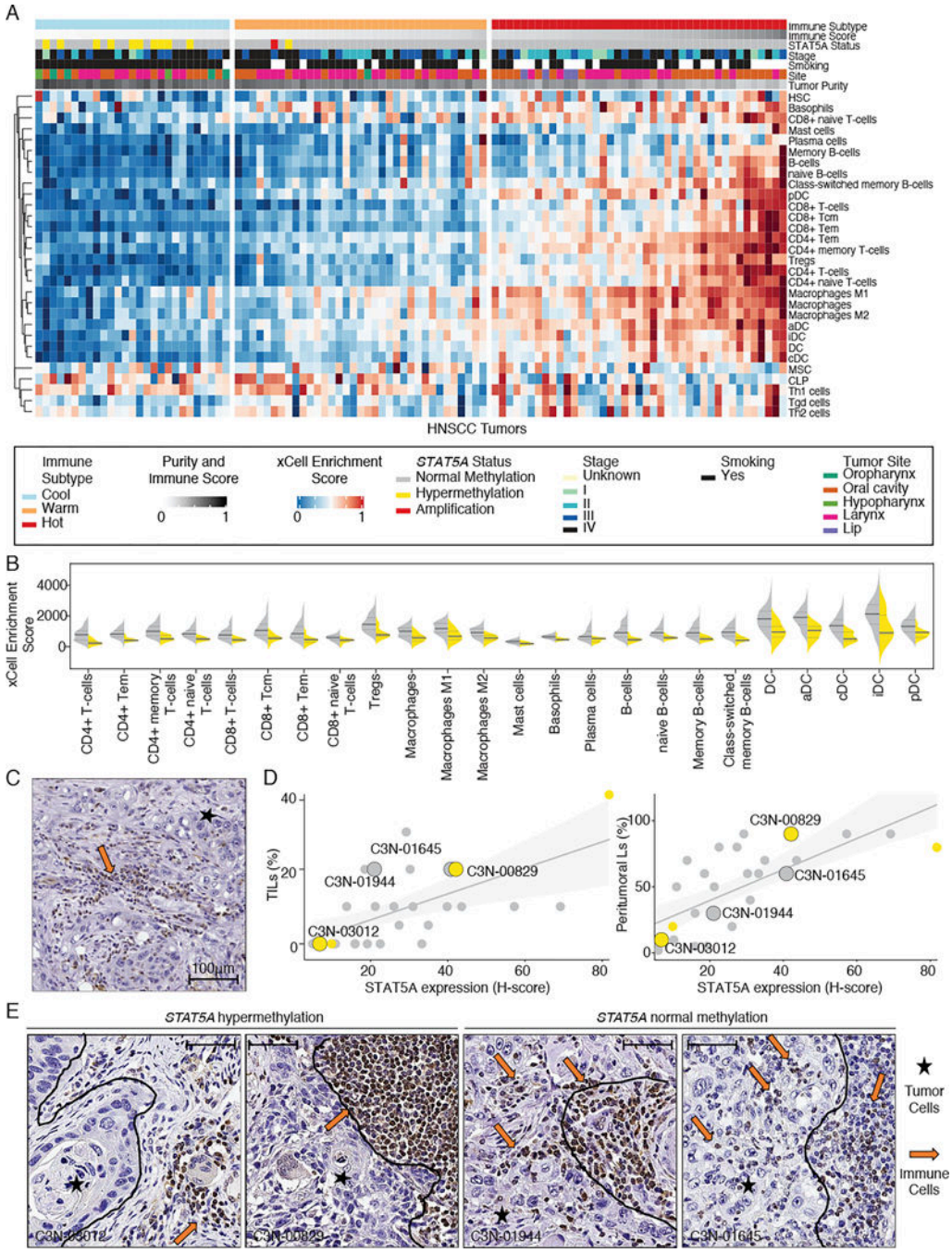

Figure 6. Functional impact of *STAT5A* hypermethylation on immune cell depletion in HNSCC

(A) Heatmaps showing distinct immune subtypes of HNSCC tumors derived from xCell enrichment scores. The top panel shows the immune score, DNA methylation status of *STAT5A*, immune subtype, and tumor stage.

(B) Violin plots comparing xCell enrichment scores of immune effectors and dendritic cells in hypermethylated *STAT5A* (yellow) and normally methylated *STAT5A* (gray) samples in HNSCC tumors. Median values are shown as solid black lines, and first and third quartiles

are represented by dashed lines. Statistical significance was determined using a Wilcoxon rank-sum test.

(C) Representative image of IHC (immunohistochemistry) staining of STAT5A protein (brown) in HNSCC tumor sample. Scale bar = 100 μm.

(D) Correlation between the quantified STAT5A protein abundance versus the level of tumor-infiltrating lymphocytes (TILs, left panel) or peritumoral lymphocytes (right panel). Samples were colored by the DNA methylation status of STAT5A (yellow: hypermethylation, gray: normal methylation). Samples with representative IHC images are highlighted by large dot size.

(E) IHC staining of STAT5A in HNSCC tumors. Representative tumor cells (stars) and lymphocytes (arrows) are shown. Tumor boundary is indicated by a black line. Scale bar = 100 μm.

See also Figure S6 and Table S3.

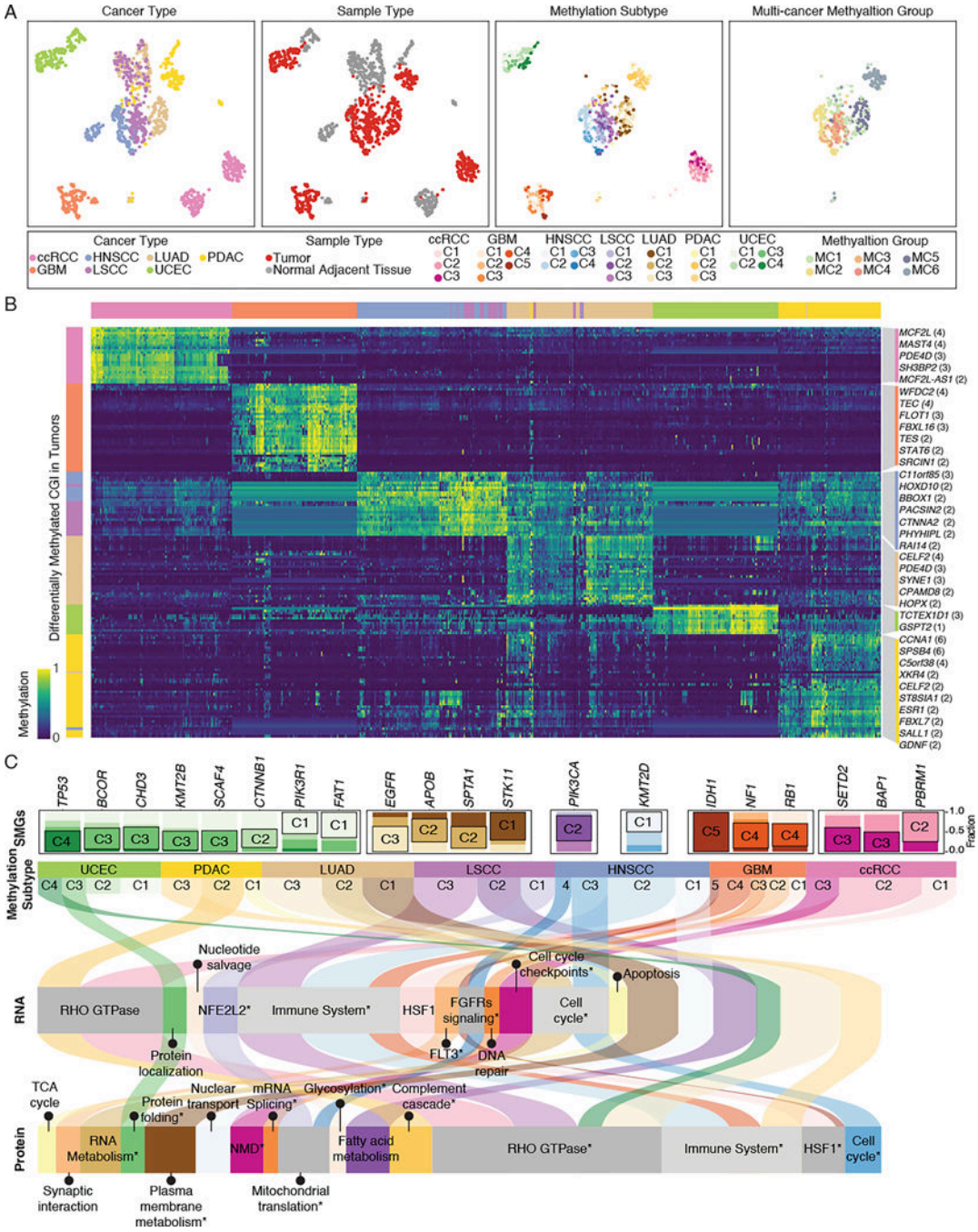

Figure 7. Summary of the cancer methylome for cell-of-origin, tumor signatures, and therapy

(A) Projection of the cancer methylomes. Each point is a sample and is colored based on the cancer type (first column), sample type (second column), methylation subtype (third column), or multi-cancer methylation group (fourth column).

(B) Heatmap of differentially methylated CpG sites at promoter regions in seven cancer cohorts compared to normal adjacent tissue. Selected promoters annotated with the number of differentially methylated CpG sites are shown.

(C) Alluvial plot showing the per-cancer methylation subtypes (second row), their enriched significantly mutated genes (SMGs) (first row), enriched RNA expression signature (third row), and enriched protein signature (fourth row). The curved lines across panels correspond to different methylation subtypes.
Signatures with FDR P-values < 0.05 are highlighted with *.
See also Figure S7 and Tables S4-S6.

Key resources table

REAGENT or RESOURCE	SOURCE	IDENTIFIER
Antibodies		
Rabbit polyclonal anti-STAT5A antibody	Atlas Antibodies	Catalog: HPA042128, RRID: AB_2677864
Biological samples		
Primary tumor and normal adjacent tissue samples	CANCER-CELL-D- 22–00603 companion Pan-Cancer resource manuscript[47]	https://pdc.cancer.gov/pdc/cptac-pancancer
Chemicals, peptides, and recombinant proteins		
Dako Protein Block, Serum-free blocking solution	Agilent Technologies Inc	Catalog: X090930–2
Dako Taget Retrieval Solution, pH=6	Agilent Technologies Inc	Catalog: S236984–2
Dako Wash Buffer 10X	Agilent Technologies Inc	Catalog: S3006
Critical commercial assays		
TruSeq Stranded Total RNA Library Prep Kit with Ribo-Zero Gold	Illumina	Catalog: RS-122–2301
Infinium MethylationEPIC Kit	Illumina	Catalog: WG-317–1003
Nextera DNA Exosome Kit	Illumina	Catalog: 20020617
KAPA Hyper Prep Kit, PCR-free	Roche	Catalog: 07962371001
TMT-11 Reagent Kit	ThermoFisher Scientific	Catalog: A34808
BCA Protein Assay Kit	ThermoFisher Scientific	Catalog: 23225
PTMScan® Acetyl-Lysine Motif [Ac-K] Kit	Cell Signaling	Catalog: 13416
EnVision FLEX Visualizing Kit	Agilent Technologies Inc	Catalog: K800221–2
Deposited data		
CIViC nightly, 062220	Griffith et al.[79]	https://civicdb.org/home
FANTOM5	FANTOM Consortium et al.[87]	http://fantom.gsc.riken.jp/5/
TARGET Methylation data	Pugh et al.[88]	https://ocg.cancer.gov/programs/target/data-matrix
TCGA Methylation data and RNA-seq data	TCGA et al.[64,71,78,89–92]	https://gdac.broadinstitute.org/
JASPAR	Khan et al.[93]	https://jaspar.genereg.net/
InfiniumAnnotation	Zhou et al.[94]	https://zwdzwd.github.io/InfiniumAnnotation
OmniPath	Türei et al.[95]	http://omnipathdb.org/
ccRCC scRNA-seq data	Li et al.[25]	https://portal.gdc.cancer.gov/projects/CPTAC-3
GBM scRNA-seq data	Wang et al.[24]	https://portal.gdc.cancer.gov/projects/CPTAC-3
PDAC scRNA-seq data	Cui Zhou et al.[26]	https://data.humantumoratlas.org/
Lungs scRNA-seq data	Travaglini et al.[27]	https://www.synapse.org/#!Synapse:syn21041850
CPTAC clinical and proteomic data	CANCER-CELL-D- 22–00603 companion Pan-Cancer resource manuscript[47]	https://pdc.cancer.gov/pdc/cptac-pancancer

REAGENT or RESOURCE	SOURCE	IDENTIFIER
CPTAC genomic and transcriptomic data	CANCER-CELL-D- 22–00603 companion Pan-Cancer resource manuscript[47]	https://pdc.cancer.gov/pdc/cptac-pancancer and Cancer Data Service (CDS)
CPTAC DNA methylation data	This study	https://pdc.cancer.gov/pdc/cptac-pancancer
CPTAC acetylation data	CANCER-CELL-D- 22–00603 companion Pan-Cancer resource manuscript[47]	https://pdc.cancer.gov/pdc/cptac-pancancer
Software and algorithms		
RESET	Saghafinia et al.[9]	http://ciriellolab.org/reset/reset.html
ChAMP	Morris et al.[96]	https://www.bioconductor.org/packages/release/bioc/vignettes/ChAMP/inst/doc/ChAMP.html
Methylation array analysis pipeline for CPTAC	This study	https://github.com/ding-lab/cptac_methylation
methylationArrayAnalysis v3.9	Maksimovic et al.[97]	https://master.bioconductor.org/packages/release/workflows/html/methylationArrayAnalysis.html
Illumina EPIC methylation array v0.6	See link	https://bioconductor.org/packages/release/data/annotation/html/IlluminaHumanMethylationEPICanno.ilm10b2.hg19.html
ConsensusClusterPlus v1.48.0	Wilkerson et al.[98]	https://bioconductor.org/packages/ConsensusClusterPlus/
xCell v1.2	Aran et al.[45]	http://xcell.ucsf.edu/
SomaticWrapper	Ding Lab	https://github.com/ding-lab/somaticwrapper
Strelka2	Saunders et al.[99]	https://github.com/Illumina/strelka
MUTECT v1.1.7	Cibulskis et al.[100]	https://software.broadinstitute.org/gatk/download/archive
VarScan v2.3.8	Koboldt et al.[101]	http://varscan.sourceforge.net
Pindel v0.2.5	Ye et al.[102]	http://gmt.genome.wustl.edu/packages/pindel/
Fusion calling pipeline for CPTAC	Gao et al.[103]	https://github.com/cuidaniel/Fusion_hg38
STAR-Fusion v1.5.0	Haas et al.[104]	https://github.com/STAR-Fusion/STAR-Fusion/wiki
EricScript v0.5.5	Benelli et al.[105]	https://sites.google.com/site/bioericscript
Integrate v0.2.6	Zhang et al.[106]	https://sourceforge.net/p/integrate-fusion/wiki/Home/
Copy Number Variant Calling	Ding Lab	https://github.com/ding-lab/BICSEQ2
BIC-seq2	Xi et al.[107]	http://compbio.med.harvard.edu/BIC-seq/
SomaticSV	Ding Lab	https://github.com/ding-lab/SomaticSV
Manta v1.6.0	Chen et al.[108]	https://github.com/Illumina/manta
MSFragger v3.4	Kong et al.[109]	https://msfragger.nesvilab.org/
Philosopher toolkit v4.0.1	da Veiga Leprevost et al.[110]	https://philosopher.nesvilab.org/
TMT-Integrator	Djomehri et al.[111]	http://tmt-integrator.nesvilab.org/
HTSeq v0.11.2	Anders et al.[117]	https://htseq.readthedocs.io/en/master/
DreamAI	Ma et al.[112]	https://github.com/WangLab-MSSM/DreamAI
ProteintPaint Lollipop	Zhou Lab	https://viz.stjude.cloud/zhou-lab/visualization/proteintpaint-lollipop-example~57
LIMMA v3.36 (R Package)	Ritchie et al.[113]	https://bioconductor.org/packages/release/bioc/html/limma.html
HOMER	Heinz et al.[114]	http://homer.salk.edu/homer/

REAGENT or RESOURCE	SOURCE	IDENTIFIER
QuPath v0.3.2	Bankhead et al.[115]	https://qupath.github.io/
Reactome	Fabregat et al.[116]	https://reactome.org/
Scanpy v1.7.0	Wolf et al.[117]	https://github.com/scverse/scanpy
Python v3.7	Python Software Foundation	https://www.python.org/
R v3.6	R Development Core Team	https://www.R-project.org/
Bioconda	Grüning et al.[118]	https://bioconda.github.io/
Bioconductor v3.9	Huber et al.[119]	https://bioconductor.org/